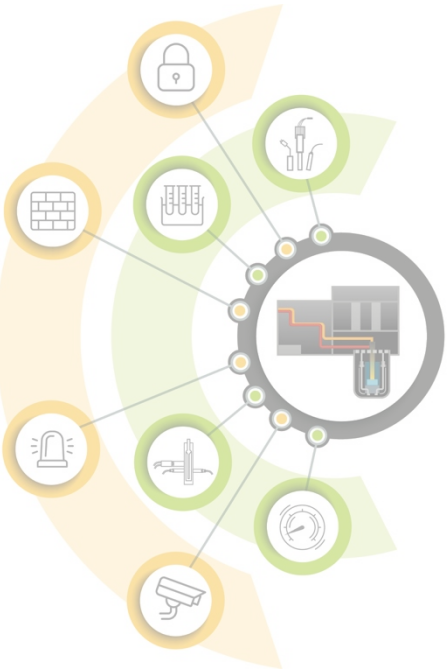

Experimental Validation of Nondestructive Assay Capabilities for Molten Salt Reactor Safeguards

FY21 Report

Prepared for

US Department of Energy

Athena Sagadevan, Daniela Henzlova, Howard Menlove, Mark Croce

Los Alamos National Laboratory

Michael Dion, Robert Morris, Bruce Bevard

Oak Ridge National Laboratory

September 30, 2021

LA-UR-21-29908

ORNL/TM-2021/2288

1. Introduction

Current molten salt reactor (MSR) safeguards modeling efforts are limited by the lack of measurement data on realistic MSR materials as identified by advanced nuclear industry leaders and safeguards modeling experts. The challenging environment of an MSR where accessibility or direct sampling may be limited or impossible means that rapid, non-destructive characterization of fissile material and waste streams at MSRs is likely to be essential to meet regulatory requirements in a cost-effective way. An advanced systems approach is needed to meet safeguards requirements, and a main component of this approach is validated measurement performance capabilities. The goal of this project is to (1) measure gamma-ray and neutron signatures from nuclear material samples that have characteristics similar to material at an MSR facility, (2) assess limits of rapid anomaly detection and characterization of material compositions, and (3) evaluate nondestructive assay (NDA) concepts for harsh, high-radiation environments.

The experimental approach is based on a series of measurement campaigns using traditional and advanced NDA technologies to comprehensively evaluate performance with respect to material composition, spectral complexity, dose rate, cooling time, measurement environment, and other unique challenges of MSR facilities.

In FY20, a systematic approach was developed for the evaluation of NDA measurement capabilities and applied to a measurement campaign at Los Alamos National Laboratory focused on gamma-ray measurement technology. Measured materials from a spent fuel separation process at Argonne National Laboratory were chosen to evaluate limits of quantifying fissile material signatures in the presence of varying concentrations of fission products and actinides. Both HPGe and microcalorimetry are capable of quantifying important nuclides, and each have unique advantages due to efficiency or energy resolution. Results suggest that direct quantification of important actinides in fuel salt may be possible by NDA for a sampling loop in an operating MSR or for salt samples.

FY21 work focused on validation of neutron detector performance in realistic operational environments including the Oak Ridge National Laboratory Irradiated Fuels Examination Facility (IFEL). For the scope of this work, the Molten Salt Demonstration Reactor (MSDR) is chosen as our design basis reactor. The MSDR was chosen as it had widely available literature that was well documented for developing a process model. This reactor model will provide an initial estimate of MSR-like fuel material to understand the expected neutron and gamma characteristics of the MSR fuel salt that will be used as an input to design experiments for neutron NDA technology testing.

MSDR is a conceptual 750 MWth molten salt reactor that was designed based on the legacy Molten Salt Reactor Experiment. The MSDR design is coupled with SCALE, a comprehensive modeling and simulation suite for nuclear safety analysis to perform analysis of the MSR salt. The SCALE modeling was performed by Sandia National Laboratory (SNL) [1] and the results of this modeling were used in this report to estimate neutron and gamma-ray emission characteristics representative of MSR fuel salt. The details of the SCALE modeling results and the corresponding expected neutron and gamma-ray characteristics will be discussed in the following sections.

2. Overview of MSR fuel Composition

The initial composition of the MSDR fuel used in the SCALE model is listed in Table 1. The fuel is a LiF - UF_4 salt containing low enriched uranium (LEU) with 5% enrichment. The assumed operating conditions of the reactor involve continuous fission product gas removal, continuous fission product metal removal (Se, Nb, Mo, Tc, Ru, Rh, Pd, Ag, Sb, Te), and continuous feed additions (flow was optimized to maintain ^{238}U inventory).

The MSDR with this fuel salt will have about 121 metric tons of heavy metal (MTHM) within 195 metric tons of fuel salt. In order to design experimental conditions to mimic MSR salt characteristics for evaluation of neutron detection technologies, it is necessary to extract the expected neutron and gamma-ray emission characteristics. For this reason, a unit measure of 100 g of MSDR fuel salt was analyzed and will be used for all the calculations of neutron and gamma-ray emission characteristics within this report. The SCALE MSDR model assumed salt irradiation of 8 years, as per the design, which plans to replace the primary salt after that time.

Table 1: Initial MSDR fuel composition.

Isotope	ZAID	Weight Fraction	Mass Density [g/cm^3]
^{6}Li	3006	0.000002	0.000011
^{7}Li	3007	0.048358	0.227764
^{19}F	9019	0.329642	1.552612
^{235}U	92235	0.030789	0.145016
^{238}U	92238	0.591210	2.784597
Total	-	1.000000	4.710000

The goal of the present project is to evaluate representative neutron NDA technologies to inform future development of safeguards approaches for the MSR fuel over its lifecycle. This is a complex problem as MSR fuel composition will be dynamically changing throughout the irradiation and additionally the Pu neutron signatures can be obscured by the contribution from other actinides (e.g. Cm) and neutrons from (α,n) reactions.

To evaluate MSDR material characteristics, neutron and gamma-ray emissions were evaluated for 100 g of fuel salt based on the SCALE modeling results of concentrations (g/MTHM) of the key isotopes with dominant contributions to the neutron and gamma-ray signals. Additionally, contributions from spontaneous fissions and (α,n) reactions to the total neutron emission from this material were evaluated to obtain a more complete understanding of the expected neutron signatures.

2.1. Neutron and gamma emissions from MSR spent fuel

SNL provided SCALE results for the MSDR [1] for a reference case of the regular operation of the MSDR for 8 years. The spent fuel salt at 8 years of burnup is highly radioactive with significant neutron and gamma emissions. The material is closely studied in order to make informed decisions for the neutron NDA measurement campaign. Since MSR fuel is not readily available for experiments, knowing detailed information regarding the fuel composition is pertinent to the design of the experiment. Ultimately, we want to study the safeguardability of this fuel using neutron NDA techniques, hence accurately modeling the fuel composition and interpreting that data will allow us to perform experiments in similar conditions and determine the detector response, which ultimately decides if declared properties of this fuel can be independently verified, i.e. "safeguarded".

The major contributors to neutron emission are from nuclei undergoing spontaneous fission and those intense alpha emitters that lead to significant contribution through (α,n) reactions. Isotopes with high spontaneous fission neutron yields, present in the MSDR fuel salt, include ^{238}Pu, ^{240}Pu, ^{242}Pu, ^{242}Cm, ^{244}Cm. The spontaneous fission neutron emission rate from 100 g of MSDR fuel salt was calculated using spontaneous neutron fission yield for each isotope [2] and the corresponding mass of each isotope obtained from the SCALE calculation. ^{242}Cm and ^{244}Cm have the highest spontaneous fission neutron yields (2.1×10^{7} n/s-g and 1.08×10^{7} n/s-g, respectively) and therefore, despite being present in minute fractions (3.47×10^{-4} g and 5.39×10^{-5} per 100 g sample, respectively), they provide dominant contribution to neutron emission rate from spontaneous fission. ^{238}U on the other hand, has a low spontaneous fission neutron yield (1.36×10^{-2} n/s-g) but is abundantly present (59.2 g per 100 g sample) thus also significantly contributing to spontaneous fission neutron emissions. As expected from the LEU composition of the input fuel salt, the most prominent spontaneous fission neutron contributors for the MSDR material are ^{242}Cm, ^{244}Cm and Pu isotopes. A detailed overview of these contributions is summarized in Figure 2 and Table 3 below.

In majority of actinides, α-decay is far more probable than spontaneous fission. The interaction of α particles with light elements (F, Li) present in the fuel salt will lead to significant neutron emission from (α,n) reactions due the large concentration of these light elements. The (α,n) neutrons can be comparable in number to spontaneous fission neutrons if isotopes with high α decay rates are present. Based on the SCALE modeling results, the isotopes with highest α yield present in the MSDR fuel salt include ^{242}Cm, ^{244}Cm, ^{241}Am, ^{238}Pu, ^{239}Pu, and ^{240}Pu. To quantify the neutron emission rate from (α,n) reactions for the MSDR material, the code Sources4c was utilized. Sources4c is a code system that determines neutron production rates and spectra from (α,n) reactions, spontaneous fission, and delayed neutron emission due to radionuclide decay [3]. Sources4c calculations used the isotopic concentrations and MSDR salt composition provided by the SCALE modeling as an input. The presence of the light elements such as fluorine and lithium in the MSDR salt will yield orders of magnitude more neutrons than in case of commercial light water reactor (LWR) fuel where the most abundant light element is oxygen. Note that the neutron yield from (α,n) reaction on fluorine corresponds to 5.9 per 10^{6} 5.2 MeV α-particles, whereas for oxygen it is only 0.059 neutrons per 10^{6} 5.2 MeV α-particles [1]. Table 2 summarizes total neutron emission rates for 100 g of MSDR fuel salt at 8 years of burnup from (α,n) reaction on the key light elements present in this material. It can be seen that (α,n) interactions on fluorine represent the dominant

contribution to neutron emission from (α,n) reactions. Such significant contribution of (α,n) neutrons in MSDR fuel salt will pose a challenge for safeguarding this material.

Table 2: Isotopic breakdown of neutron emission rates from (α,n) reactions on the key light elements present in MSDR fuel salt (results shown are for 100 g of MSDR fuel salt at 2880 days of burnup).

Isotope	**neutron emission rate from (α,n) reactions [n/s]**		
	^{19}F	**^{7}Li**	**^{18}O**
^{242}Cm	4.13E+05	2.99E+04	1.17E-04
^{239}Pu	4.28E+03	1.65E+02	1.64E-06
^{240}Pu	3.10E+03	1.21E+02	1.19E-06
^{238}Pu	7.53E+03	3.86E+02	2.55E-06
^{241}Am	3.91E+03	2.00E+02	1.33E-06
^{244}Cm	1.22E+03	7.29E+01	3.77E-07
^{241}Pu	1.51E+01	3.22E-01	6.61E-09
^{238}U	6.65E-01	0.00E+00	4.32E-10
^{236}U	8.02E-01	1.25E-03	4.38E-10
^{235}U	2.16E-01	1.69E-04	1.24E-10
^{242}Pu	2.74E+00	5.79E-02	1.20E-09
Total	**4.33E+05**	**3.09E+04**	**1.24E-04**

A detailed overview of the neutron emission rates from (α,n) reactions is presented in Figures 1-2 and Table 3 below. Figure 1 illustrates the total (α,n) and spontaneous fission neutron emission rates calculated for the MSDR fuel at various points throughout its cycle, corresponding approximately to 1/3, 2/3 and the end of the lifecycle of the reactor. This translates to 936 days, 1944 days and 2880 days of operation. It can be seen that the neutron contribution from (α,n) reactions is approximately 2 orders of magnitude larger than neutron emission rate from spontaneous fissions throughout the entire reactor lifecycle. When considering safeguards measures for this reactor type, the Pu content in the fuel salt is one of the greatest interest. To fully evaluate safeguardability of this type of reactor and assess feasibility of neutron NDA technology to evaluate Pu content, it is therefore of paramount importance to understand contribution of individual isotopes to the total neutron emission rate. This information is summarized in Figure 2 and Table 3 below.

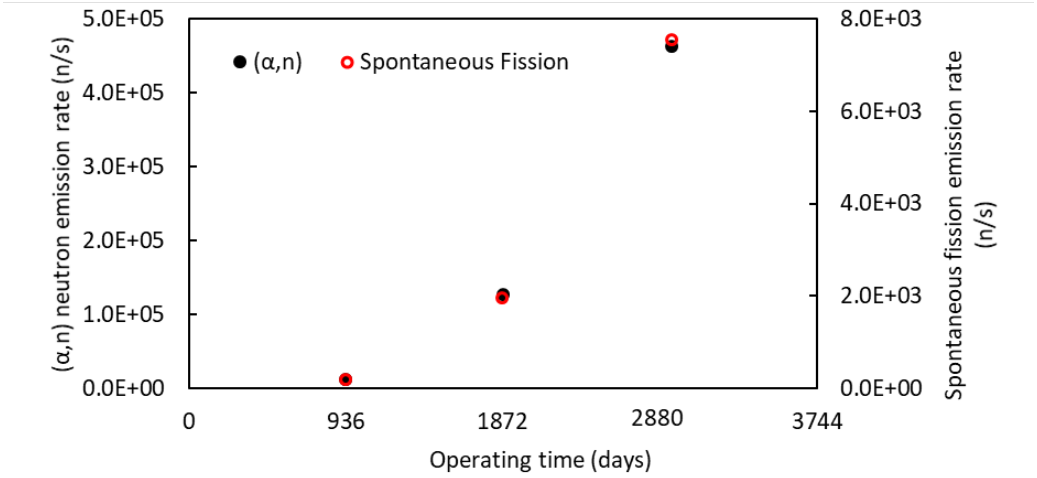

Figure 1: (α,n) and spontaneous fission neutron emission rates calculated for 100 g of MSDR fuel salt at various points throughout the reactor lifecycle.

Figure 2 and Table 3 show the isotopic breakdown of the spontaneous fission and (α,n) neutron emission rates for 100 g of MSDR fuel salt at 936, 1872 and 2880 days (8 years). Of the light elements present in the fuel salt, (α,n) reactions on ^{19}F yield the highest number of neutrons as shown in Table 2. The results presented below therefore correspond to (α,n) neutron emission rates calculated by Sources4c for the interactions with ^{19}F. From Figure 2 and Table 3 it can be seen that the primary contribution to total spontaneous fission neutron emission rate is from ^{242}Cm and ^{244}Cm isotopes for all points throughout the MSDR reactor lifecycle. In fact the spontaneous neutron emission rate from ^{242}Cm is almost 2 orders of magnitude higher than that from the strongest contributing Pu isotope (^{240}Pu). Due to its short half life (163 days), ^{242}Cm does not typically provide significant contribution to neutron emissions in the present-day LWR spent fuel assemblies due to the long cooling times typically required before the fuel is handled for processing or long term storage. However, most MSR fuel cycle concepts assume online refueling and reprocessing to maximize achievable burn-ups and reactor performance and enable closed fuel cycle. It is therefore essential to be able to assay MSR fuel material during the reactor operation with minimal cooling times. Spontaneous fission from ^{242}Cm will therefore provide an essential contribution to detected neutron signatures from MSR fuel salt and complicate assay of Pu content of this material.

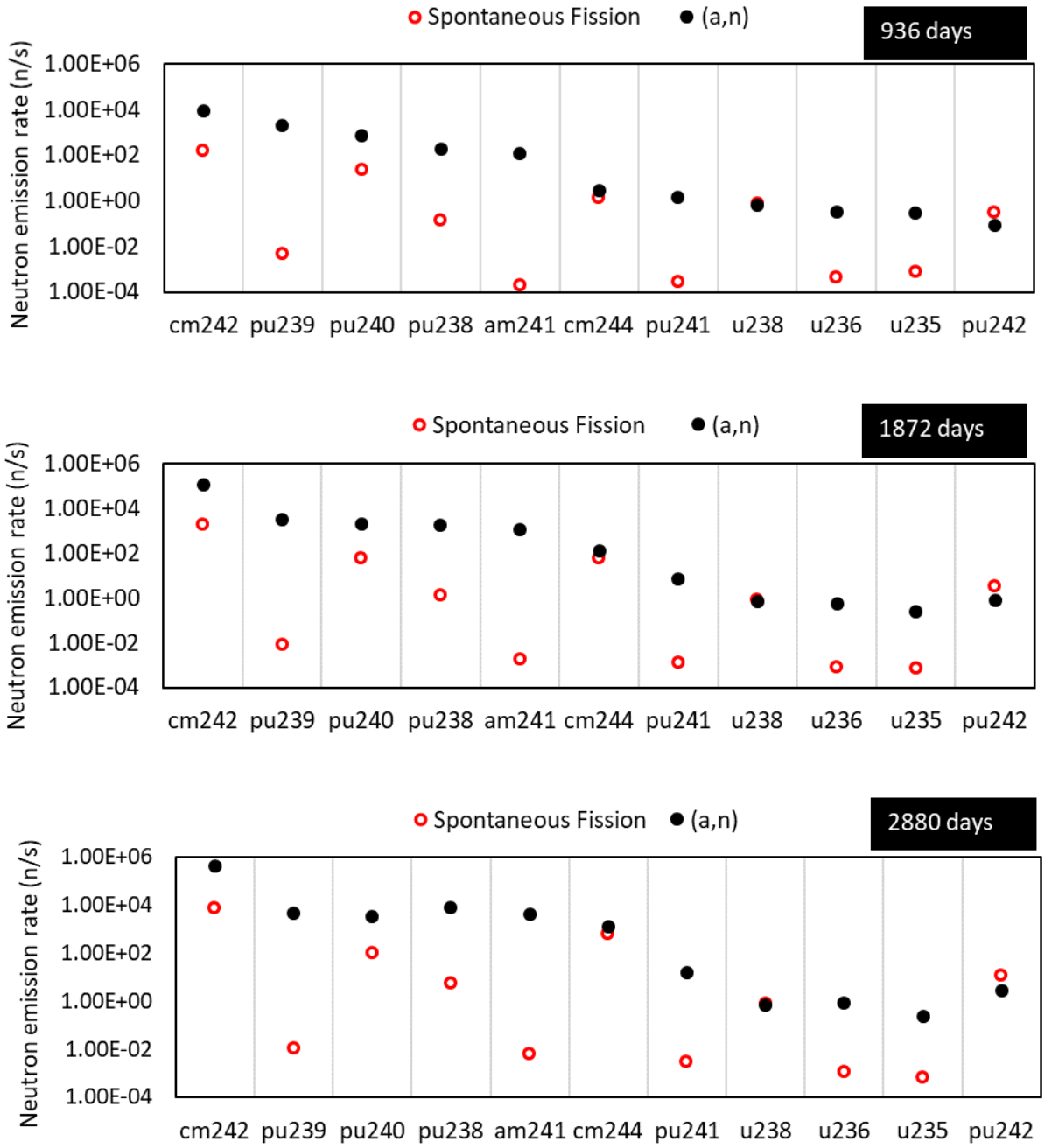

Figure 2: The isotopic breakdown of the spontaneous fission and (α,n) neutron contributions from the 100 g of MSDR fuel salt at 936, 1872 and 2880 days of reactor operation.

Additionally, as indicated in Figure 1, neutrons from (α,n) reactions will dominate neutron emissions from MSDR fuel salt for all points throughout the reactor lifecycle. This is also confirmed in Figure 2 and Table 3 where neutron emission from (α,n) reactions clearly exceeds neutron emission rates from spontaneous fissions for nearly all key spontaneous fission isotopes.

Table 3: Isotopic breakdown of neutron emission rates from (α,n) reactions and spontaneous fission for burnups of 936 days, 1872 days and 2880 days respectively.

Isotope	Neutron emission rate from (α,n) [n/s]			Spontaneous fission neutron emission rate [n/s]		
	936 [days]	1872 [days]	2880 [days]	936 [days]	1872 [days]	2880 [days]
^{242}Cm	8.65E+03	1.11E+05	4.13E+05	1.53E+02	1.95E+03	7.29E+03
^{239}Pu	1.96E+03	3.25E+03	4.28E+03	4.73E-03	7.86E-03	1.04E-02
^{240}Pu	7.28E+02	1.90E+03	3.10E+03	2.23E+01	5.81E+01	9.45E+01
^{238}Pu	1.92E+02	1.77E+03	7.53E+03	1.38E-01	1.27E+00	5.41E+00
^{241}Am	1.21E+02	1.15E+03	3.91E+03	1.98E-04	1.89E-03	6.44E-03
^{244}Cm	2.83E+00	1.30E+02	1.22E+03	1.35E+00	6.19E+01	5.82E+02
^{241}Pu	1.42E+00	6.74E+00	1.51E+01	2.66E-04	1.26E-03	2.82E-03
^{238}U	6.64E-01	6.65E-01	6.65E-01	8.04E-01	8.05E-01	8.05E-01
^{236}U	3.14E-01	5.69E-01	8.02E-01	4.44E-04	8.06E-04	1.13E-03
^{235}U	2.78E-01	2.45E-01	2.16E-01	8.03E-04	7.09E-04	6.25E-04
^{242}Pu	8.08E-02	7.79E-01	2.74E+00	3.28E-01	3.17E+00	1.11E+01
Total	**1.17E+04**	**1.19E+05**	**4.33E+05**	**1.78E+02**	**2.08E+03**	**7.98E+03**

From the above evaluation of neutron characteristics of MSDR fuel salt it is clear that LEU fueled MSR salt will pose significant safeguards challenges as the Pu neutron emissions will be largely obscured by the Cm and (α,n) neutron emissions. In order to access the Pu content in the MSR salt using neutron NDA, further evaluation will be performed during FY22, focusing on techniques such as correlated neutron counting or Cm-ratio. The Pu to Cm ratio technique was developed to quantify Pu content in present-day spent fuel reprocessing facilities, where the neutron emissions are dominated by spontaneous fissions of ^{244}Cm. The Cm/Pu ratio is typically obtained by performing destructive analysis (DA) on a sample taken from the feed materials [2]. In case of MSR, the Cm/Pu ratio will be dynamically changing throughout the reactor lifecycle, as illustrated in Table 4. Therefore, in order to potentially employ this technique for MSR safeguards Cm/Pu ratio would have to be established for sample representative of material to be measured by NDA technique.

Table 4: Cm/Pu ratio extracted from neutron emission rates calculated for 100 g of MSDR fuel salt for three different points throughout the reactor lifecycle.

Operating time [days]	Cm/Pu ratio
936	6.8
1872	32.2
2880	70.9

In addition to neutron emission characteristics, gamma-ray emissions are also essential for assessment of neutron NDA techniques to assure that neutron signal can be reliably measured and distinguished from

gamma-ray background. In present-day LWR spent fuel, the gamma-ray emissions are dominated by ^{137}Cs due to the short half lives of majority of the gamma emitting fission products. Nevertheless, as outlined earlier, in order to assure monitoring and verification of MSR reactor it is expected that material assay will be performed during the MSR operation. The contribution of short-lived fission products to gamma-ray emissions therefore will have to be taken into account. Analysis of the MSDR SCALE results indicates that in addition to ^{137}Cs there is a range of isotopes with half lives greater than at least tens of minutes that will likely contribute to gamma-ray emissions if measurements are performed on MSR fuel salt sample. The dominant contributions will include ^{140}La, ^{95}Zr, ^{97}Zr, ^{97}Nb, ^{133}I and ^{135}I. Gamma dose rate for 100 g of MSDR fuel salt from ^{137}Cs corresponds to ~100 R/h at 10 cm, however due to the high activity of short-lived fission products predicted by SCALE, significantly higher dose rates (thousands of R/h) can be expected for this material if measured shortly after removal from reactor. In order to assess neutron NDA for MSR applications it is therefore essential to evaluate neutron NDA techniques performance in high gamma-ray environments.

The above analysis provides useful insight into the neutron and gamma-ray emission characteristics of representative MSR fuel salt. These calculations were performed in order to be able to design experiments mimicking these characteristics to evaluate neutron NDA techniques performance for MSR fuel salt materials. In summary, a case study for 100 g fuel sample at 8 years of reactor operation and no cooling time indicated total neutron emission rate of ~5E+05 n/s. Gamma dose rates in the MSR applications are expected correspond to 1000s of R/h. Since MSR fuel is not available for experiments, this information is crucial to design experiments to assure MSR-type measurement conditions and was used to inform experimental campaigns described in Section 4 and 5 of this report.

3. Evaluated neutron NDA techniques

To fully evaluate neutron NDA capabilities for MSR applications, this work focuses on inter-comparison of several neutron detection techniques, which include detectors used in present day safeguards applications as well as a novel neutron detection instrument developed specifically for high gamma dose environments. A comprehensive evaluation of all the detectors will allow for benchmarking the best detection technology for this application and comparing individual performances.

The neutron detection technologies traditionally used in safeguards applications include primarily ^{3}He-based proportional counters and fission chambers. ^{3}He-based instruments have been a gold standard of nuclear safeguards for the past decades and provide high neutron detection efficiency to support quantitative nuclear material assay. Fission chambers are typically used in applications with high gamma dose rates, such as spent fuel measurements and are capable of operating at dose rates of 10^{6}-10^{7} R/h, however they provide very low detection efficiency on the order of 0.01%. Additionally, the fission chambers present shipping and regulatory control issues because of the fissile material content.

The new technology developed for high gamma background applications, such as MSRs, used in this evaluation is the mini High Dose Neutron Detector (miniHDND). The miniHDND technology is based on boron-lined proportional counters, which provide inherent fast signal characteristics and high gamma dose tolerance [4]. In addition, the miniHDND provides capability of simultaneous neutron and gamma-ray monitoring capability. Individual detectors used in this work are shown in Figure 3.

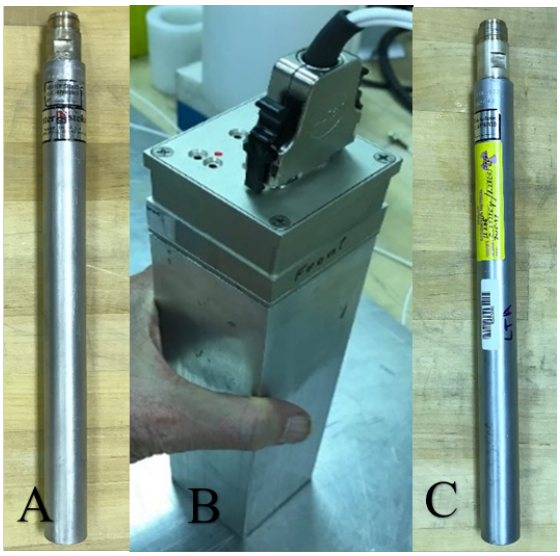

Figure 3: Neutron detectors considered in this work - A: ^{3}He detector, B: miniHDND and C: fission chamber.

As discussed in the previous section, gamma-ray dose rates of 1000 R/h or more are expected for samples (100 g assumed in this work) of MSR material. The gamma-ray sensitivity of each neutron detection technology will therefore need to be evaluated.

Gamma rays can transfer energy to electrons by Compton scattering or photoelectric effect in the detector fill gas or the walls yielding high-energy electrons that in turn produce a column of ionization as they traverse the detector. Hence, when choosing a ^{3}He detector for high gamma background applications, the detector wall material, gas pressure and quench as are important considerations. For sufficiently high gamma dose rates, electronic pulses induced by gamma rays can pile-up within the resolving time of the signal processing electronics to yield pulses comparable to neutron pulses [2]. Typically ^{3}He detectors are filled at 4 atm pressure, but higher pressures are also often used to increase thermal neutron detection efficiency. However, when immersed in a high gamma field, the detector at higher fill pressure becomes more vulnerable to gamma pile-up. In order to show this effect and demonstrate more broadly the expected ^{3}He performance in high gamma dose environments for MSR applications, two ^{3}He detectors with different fill gas pressures were selected in this work. Detector ^{3}He_1 is pressurized to 4 atm, has an aluminum shell and uses CO_2 as the quench gas. The diameter of the detector is 1” with 12” active length. Detector ^{3}He_2 has the same shell material and quench gas, but is pressurized to 9 atm and its active length corresponds to 11”. Note that in order to assure fair comparison among all the detection technologies evaluated in this work, additional 1 mm layer of Cd is used to unify the active length for all detectors. The reference active length, corresponding to the shortest system evaluated in this study, is 8.8”.

The wall material and quench gas of ^{3}He detectors are the additional important criteria to consider when selecting ^{3}He detectors for in high gamma dose environments. ^{3}He detectors are typically encased in aluminum or stainless steel. Stainless steel offers an advantage of superior structural strength and stainless steel walls are typically made thinner than aluminum walls as less material is required for the

same structural strength and due to stainless steel higher thermal neutron absorption cross section. However, stainless steel results in increased rate of gamma-ray interactions in the detector wall due to its higher Z (atomic number) than aluminum, which increases gamma pile-up in high gamma-ray backgrounds [5]. Thus, aluminum tubes are preferred for high gamma dose environments expected in MSR applications.

Quench gas makes up a small fraction of the composition within the ^{3}He detector, but serves many functions. The type of quench gas chosen affects the electron drift velocity, the range of the charged particles and offers a quenching mechanism that shortens the avalanche process that improves the pulse-height resolution. It is common to use polyatomic gasses such as Ar+CH_4, CF_4, CO_2 or N_2 as the quench gas in ^{3}He detectors. In high gamma dose environments, quench gasses with high Z such as Argon have poor performance [5], hence for these environments, low-Z quench gasses are better. For the considerations in this work, ^{3}He detector with CO_2 quench gas was selected as it offers fast timing compared to N_2 and very good performance in a high gamma dose environment [5].

Second detector technology used in this evaluation is miniHDND, which represents a novel technology with several advanced features. The key advantage for this application is in its improved gamma dose tolerance compared to ^{3}He [4]. As mentioned, it is based on boron-lined proportional counters. Thermal neutron detection in boron-lined proportional counter is based on $^{10}B(n,\alpha)^{7}Li$ reaction, which results in higher energy reaction products (2.3 MeV reaction energy) than in case of ^{3}He (765 keV reaction energy). The pulse height spectrum from boron-lined detector therefore results in a high energy tail that allows for improved energy discrimination to prevent gamma-ray pileup in high dose environments compared to ^{3}He detectors and extends thus the ability to attain a useable neutron signal. Additionally, miniHDND offers simultaneous measurement capability for both neutrons and gamma-rays. The internal structure of the miniHDND consists of three layers of detection cells where the front and back detection cells are ^{10}B coated for neutron detection while the middle cell is bare (not coated) and is utilized for gamma ray detection. MiniHDND includes internal layers of polyethylene between the three detection cells for neutron moderation. The thickness of polyethylene is not uniform to assure progressive neutron moderation through the layers. As discussed in Section 3.1, a dedicated polyethylene holder was also designed to provide additional neutron moderation and serve as positioning support for the instrument. MiniHDND has 2.5”x2.5” square footprint and its active length corresponds to 8.8”. Figure 6 shows a Visual Editor rendering of the miniHDND internal layout and the polyethylene holder. Another unique feature of the miniHDND is that each cell is controlled by its own amplifier module, which allows for each cell to have individualized settings to enable tuning for simultaneous neutron and gamma monitoring. Figures 9-10 in the following sections show this capability of simultaneous monitoring by measuring the high-voltage plateau for mixed neutron and gamma-ray source term at various gamma-ray dose rates.

Lastly, ^{235}U fission chamber was used in this evaluation. Fission chamber typically provides very high gamma dose tolerance, due to the high energy of fission fragments produced in neutron interactions with ^{235}U. Fission chambers therefore represent typical technology used in spent fuel applications. Fission chambers are expected to be able to withstand dose rates corresponding to 10^{6}-10^{7} R/h, however provide low neutron detection efficiency. This tradeoff is acceptable in applications that do not require high neutron detection efficiencies, such as spent fuel from commercial reactors, which provides significant neutron output. The fission chamber used in this work is 1” in diameter and its active length corresponds to 10”. It contains 0.26 g of 93% enriched uranium and is encased in Aluminum. Similarly as in case of ^{3}He detectors, for this work it is equipped with 1 mm Cd liner to provide unified active length of 8.8”.

3.1. Optimization of polyethylene moderator

The neutron detectors used in this work are thermal neutron detectors, which means that their neutron detection efficiency is a function of neutron energy and is optimum for thermal neutron energies (~0.025 eV). To optimize the neutron detection efficiency of the detectors used in this evaluation, a dedicated polyethylene moderator holder was designed in MCNP and constructed to support subsequent measurement campaigns. In addition to assuring optimum neutron moderation, to ensure fair performance comparison, the same holder design was used for all the detectors in this study.

To optimize thermal neutron detection performance, series of MCNP simulations was performed to evaluate optimum polyethylene configuration. These simulations were performed for miniHDND as well as ^{3}He detector. To establish a performance baseline for the MCNP work, an experiment was performed using bare miniHDND (i.e. with no additional external moderator) and a ^{252}Cf source (6.9E+05 n/s on Nov. 18, 2020), which was placed 11 cm from the front face of the detector (see Figure 4). The ^{252}Cf source was raised 11 cm from the table on a labjack to be positioned in the center of the miniHDND front face. In this configuration, the neutron detection efficiency of the bare miniHDHD was measured and evaluated to correspond to 0.016% ± 0.001%.

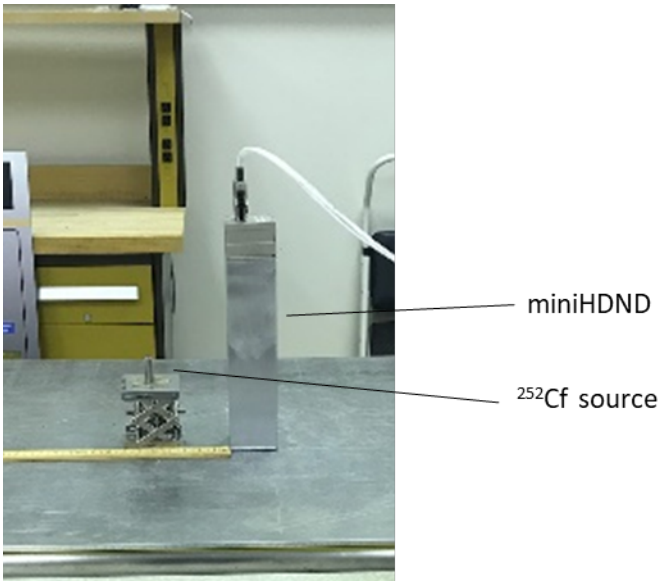

Figure 4: Experimental set-up for initial neutron detection efficiency measurement using bare miniHDND.

The MCNP simulations involved range of configurations bounded by design constrain to maintain the polyethylene height corresponding to the active length of all the compared detectors (i.e. 8.8”). The thickness of the holder was varied from 1 cm to 7 cm on the front, back and sides of the detector. Figure 5 shows the results from a set of simulations showing the optimization of the front and back polyethylene thicknesses for pre-optimized side thickness of 4 cm, which was kept unchanged in these simulations. From this set of simulations it can be seen that the optimum thickness of the front and back polyethylene was 4 cm after which increasing the polyethylene thickness produced minimal increase in neutron detection efficiency, while adding additional weight to the overall system. Therefore, 4 cm front and back

polyethylene thickness was selected as an optimum configuration and a compromise between maximum neutron detection performance and system size/weight considerations for practical handling. A visualization of the MCNP configuration for the holder with 4 cm wall thickness is shown in Figure 6.

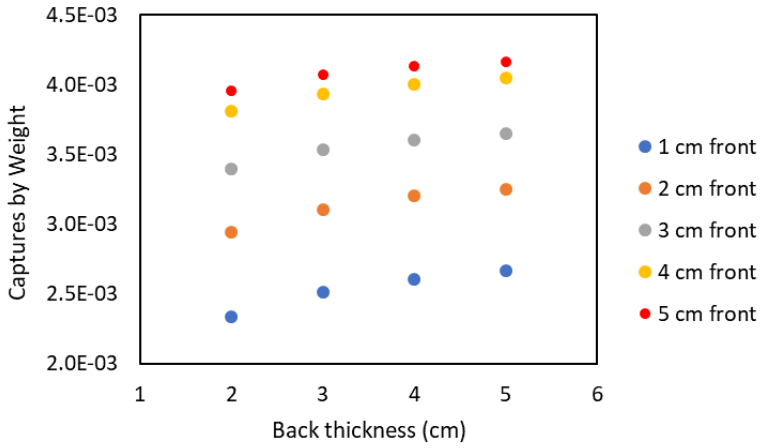

Figure 5: Results of MCNP optimization of the polyethylene holder.

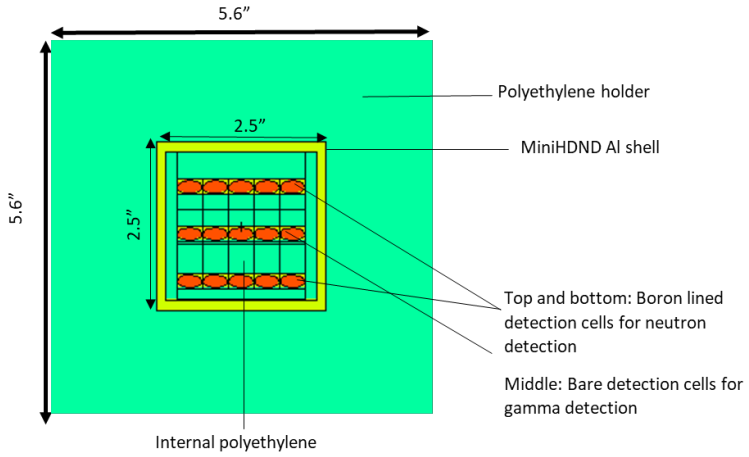

Figure 6: Visual Editor rendering of the miniHDND with external polyethylene holder used in the MCNP optimization work.

As indicated earlier, the same polyethylene holder is used also for the ^{3}He and fission chamber detectors. However, since the miniHDND has polyethylene contained inside of the detector body a dedicated polyethylene insert was designed for ^{3}He and fission chamber to compensate for this additional moderation and assure comparable neutron moderation for all three detectors. The insert was designed to fit inside the polyethylene holder 2.5”x2.5” footprint cavity and has 1” diameter opening to hold the ^{3}He and fission chamber, respectively, in place when measurements are performed. Once the MCNP optimization was finalized, a polyethylene holder and insert were fabricated and a confirmatory experiment was performed to evaluate the neutron detection efficiency of all the detectors in the new configuration including the moderator. For this experiment, a ^{252}Cf source (2.97E+05 n/s on May 5, 2021) was used. A photograph of the finished holders as well as the polyethylene insert is shown in Figure 7. As described earlier, the active length of the miniHDND corresponds to 8.8”. In order to ensure the same

active lengths were preserved for all the detection systems, cadmium sleeves were added to the ^{3}He and fission chamber detectors, which have longer active lengths (10-12”) than miniHDND, to assure the final active length corresponding to 8.8” for all the detectors. Cadmium serves as a thermal neutron absorber and will prevent thermal neutrons from reaching the cadmium covered segments of ^{3}He and fission chamber detectors. This addition allows for all the neutron detectors results to be comparable, without inherent differences of active length.

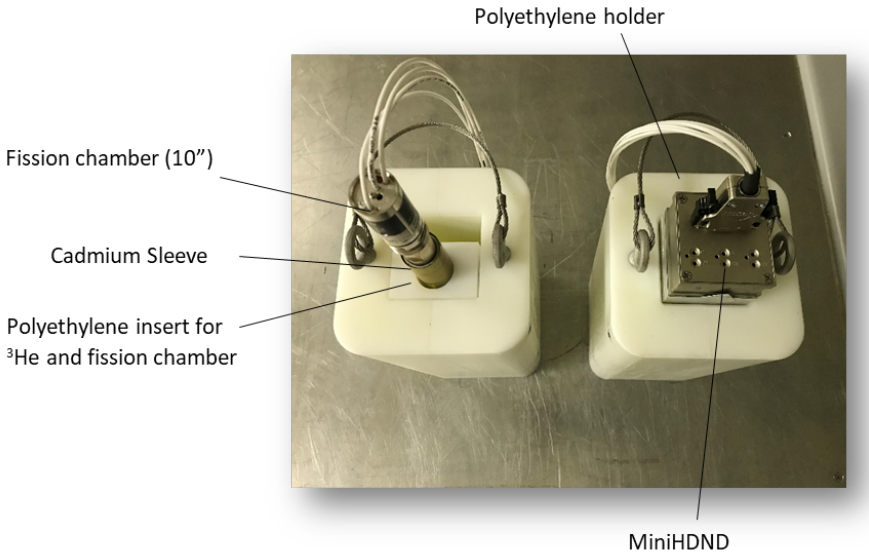

Figure 7: Photograph of the finished miniHDND and ^{3}He/fission chamber configuration using the optimized polyethylene holder with additional insert and cadmium sleeve for ^{3}He or fission chamber (left) and miniHDND inside a polyethylene holder (right).

For the miniHDND the detection efficiency was measured to be 0.15% ± 0.01%. The use of dedicated polyethylene holder therefore improved miniHDND neutron detection efficiency by almost a factor of 10. This is important for balancing neutron detection performance (i.e. assuring high neutron detection efficiency) in high gamma-ray backgrounds expected from MSR materials. Table 5 summarizes the neutron detection efficiencies for the miniHDND in the bare configuration and with a polyethylene holder as well as for the ^{3}He_1 and ^{3}He_2 and fission chamber with polyethylene holder and insert. Each of the measurements was performed at the standard operating HV setting. Note that a new optimum operating HV needs to be established for ^{3}He and boron-lined detectors specifically for high gamma dose rate environments expected in the MSR applications to prevent gamma pile-up from interfering with neutron detection. Typically, in order to assure neutron detection performance in high gamma dose environments, HV setting for ^{3}He and boron-lined detectors needs to be reduced, which simultaneously impacts their neutron detection efficiency. The magnitude of this effect on neutron detection performance in the presence of high gamma-ray backgrounds will be evaluated in the next section. Evaluation of optimum HV setting for ^{3}He and miniHDND in MSR-like gamma dose rates is key in order to enable a direct comparison of neutron detection efficiency of each of the three technologies under MSR-like conditions. Since fission chamber is capable to withstand very high gamma dose rates without impact on neutron detection performance, no adjustment of HV is needed for this detector. Fission chamber will therefore be used with its standard operating HV throughout the measurements performed within this work.

Table 5. Neutron detection efficiencies for miniHDND, ^{3}He detectors and fission chamber.

Detector and Configuration	Efficiency (%)	Uncertainty
Mini HDND - Bare	0.016	0.001
Mini HDND	0.15	0.01
3He_1	0.363	0.003
3He_2	0.426	0.004
Fission Chamber	0.007	0.001

4. High Gamma Dose Measurement Campaign

As mentioned in Section 2, for 100 g fuel sample after 8 years of MSDR operation, the neutron emission were ~5E+05 n/s and gamma emission dose rate of the order of 1000s R/h is expected. To address the high gamma dose rates expected from MSR fuel salt and evaluate necessary HV adjustment for miniHDND and ^{3}He, a dedicated experimental evaluation was designed to mimic these neutron and gamma-ray emission rates expected in MSR applications. This measurement campaign was performed at the LANL Radiation Instrumentation Calibration Facility (RIC), which houses several well characterized ^{137}Cs sources. The detectors were evaluated under various gamma dose ranging from 10 R/h up to ~700 R/h. To obtain these dose rates, ^{137}Cs sources with different activities (5 Ci, 50 Ci, 100 Ci and 1000 Ci) were used for each measurement configuration to obtain best exposure conditions coupled with varying the source detector distance. The dose rate of 693 R/h was the highest dose rate achievable from the combination of the highest source strength (1000 Ci) and minimum source detector distance that was supported by the facility configuration. The dose rate of 10 R/h was chosen as it represents typical operating limit for ^{3}He detectors with CO_2 quench gas [2]. To include the expected neutron emission from MSR-like sample a ^{252}Cf source of similar yield was used during the measurements. The available ^{252}Cf source yield corresponded to 2.76E+05 n/s (as of July 23, 2021), which is comparable to calculated neutron emission characteristics for 100 g MSDR fuel salt sample.

The setup of the experiment is shown in Figure 8 for the case of miniHDND. A laser beam was used to position the miniHDND detector such that the center of its front face was aligned with the ^{137}Cs beam (visible in Figure 8) to assure that the gamma dose rates corresponded to the detector front face and the detector location was consistent throughout the various exposures. The detector was encased in the dedicated polyethylene holder, described in Section 3, which was designed to provide improved neutron detection performance, while operating in high gamma dose environments. A ^{252}Cf source was taped to the rear of the polyethylene holder. The source was positioned on a source stand such that it was vertically in the middle of the detector. The miniHDND, polyethylene holder and ^{252}Cf source were located on a rig

that was remotely moved to various distances in order to obtain relevant dose rates. The same configuration was used also for the ^{3}He detector and fission chamber.

Figure 8: Experimental setup of miniHDND at LANL RIC facility.

To evaluate neutron detection performance of each detector in high gamma dose environment, high-voltage (HV) plateaus were measured for each gamma exposure. Figure 9 shows the typical trend in the HV plateau of miniHDND for a mixed neutron and gamma-ray source at various gamma-ray dose rates. The figure illustrates the onset of gamma pile-up beyond which the miniHDND response deviates significantly from the pure neutron case. Using such measurements, a maximum operating voltage for a given gamma dose rate can be extracted. Figure 9 demonstrates that miniHDND provides a very good ability to withstand high gamma dose rates with only a small reduction of neutron detection characteristics. This is accompanied by Table 6, which quantifies the reduction in neutron detection efficiency for the available gamma dose rates as well as reduced operating HV setting required to tolerate each gamma dose rate. Results in Table 6 were calculated for each gamma dose rate, by obtaining the neutron count rates corresponding to the point before the neutron signal begins to be affected by gamma pile-up. The miniHDND is capable to tolerate a gamma dose rate increase of almost 2 orders of magnitude (from 10 R/h to 693 R/h) with only ~26% reduction in neutron detection efficiency. This is depicted by the red dashed lines in Figure 9. As discussed previously, the ability to detect neutrons in high gamma dose environments is an essential prerequisite for successful applicability of neutron detection technology in safeguarding of MSR fuel cycle materials.

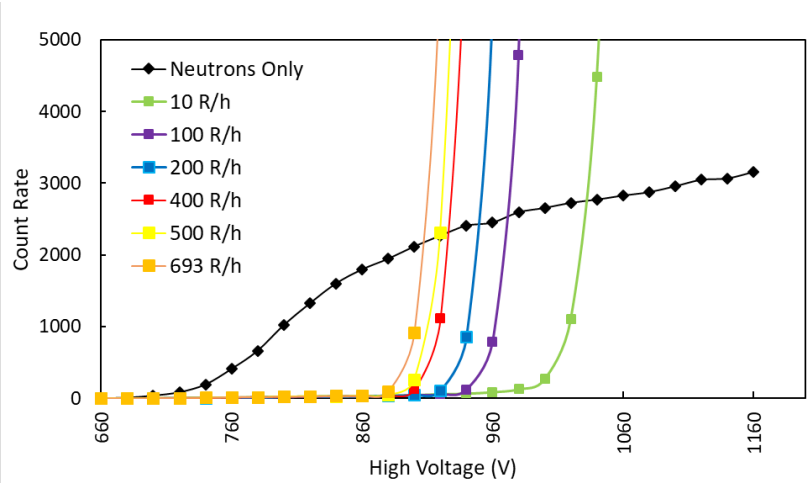

Figure 9: MiniHDND high-voltage dependance at various gamma-ray dose rates as recorded by the gamma cell compared to the neutron high voltage plateau from the neutron cells summed.

Table 6: Neutron count rate for miniHDND at various gamma dose rates available in this evaluation.

Gamma Dose Rate [R/h]	High Voltage [V]	Neutron Count Rate [cps]	σ [cps]	Percent Reduction of Neutron Detection Efficiency [%]
10	1000	2602	16	-
100	940	2317	15	11%
200	920	2220	15	15%
400	900	2080	14	20%
500	900	2122	15	18%
693	880	1931	13	26%

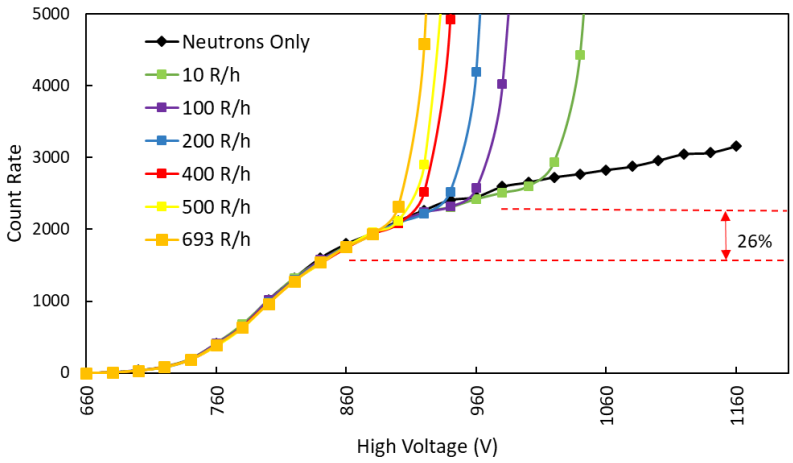

Figure 10: MiniHDND high-voltage plateau for a mixed neutron and gamma-ray source term at various gamma-ray dose rates.

Additionally, Figure 10 demonstrates the capability of the miniHDND to simultaneously measure gamma and neutron signals. The neutron detection is performed on the front and back boron-lined cells and the neutron (black) HV plateau shown in Figure 10 represents a sum of these two signals. The gamma response shown in Figure 10 is from the uncoated middle cell. Gamma response from the middle cell can be calibrated using known gamma dose rates, which would enable the miniHDND to perform gamma dose rate measurements for dose rates within the calibration range [4].

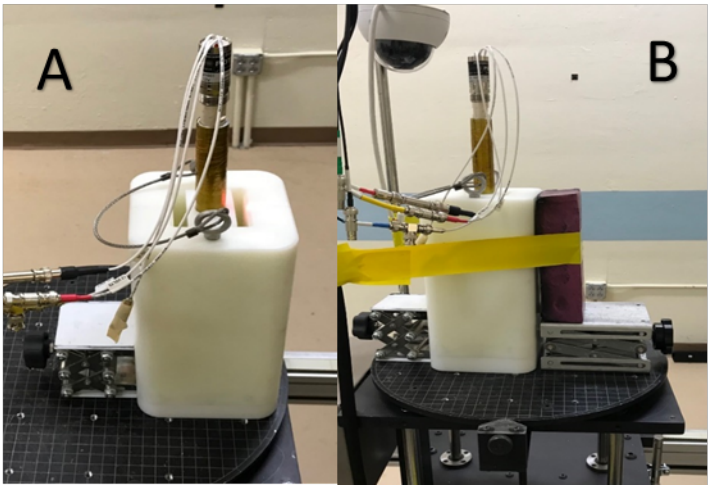

Figure 11: Experimental setup for the ^{3}He tubes (a) ^{3}He tube with no lead shielding and (b) with additional lead shielding between the detector and ^{137}Cs source.

As discussed in Section 3, two ^{3}He detectors with different fill gas pressures (4 and 9 atm, referred here as ^{3}He_1 and ^{3}He_2, respectively) were used to provide a broader assessment of neutron detection performance. Figure 11 shows the experimental setup for the ^{3}He tubes. The ^{3}He detectors were placed (one at a time) into the same polyethylene holder as miniHDND and were held in the dedicated insert to ensure the detectors maintained their position and to compensate for the additional polyethylene moderator present inside the miniHDND. Also for ^{3}He detector measurements, a laser was used to position the detectors such that their center was aligned with the ^{137}Cs source and the detector location was consistent throughout the different exposures. In order to compensate for the longer active length of these detectors compared to that of the miniHDND, the top portion, visible in Figure 11, was encased in a 1 mm thick cadmium sleeve. Two measurement configurations were tested, without (Figure 11 (a)) and with (Figure 11 (b)) an additional lead shielding. In the latter configuration, a lead brick was taped to the front of the detector, facing the ^{137}Cs source to demonstrate the effect of shielding, which would have to be used in high gamma dose environments to make the ^{3}He tube operable without (or with smaller) HV reduction and therefore with higher neutron detection efficiency. Adding lead shielding is a common practice when using ^{3}He detectors in high gamma dose applications, such as spent fuel measurements [6,7]. It provides improved gamma-ray resistance, however at the expense of increasing the overall system weight and reducing portability. The goal of the current evaluation was to compare unshielded and

shielded ^{3}He detector performance with miniHDND, which does not require lead shielding to tolerate ~700 R/h dose rates similar to MSR applications.

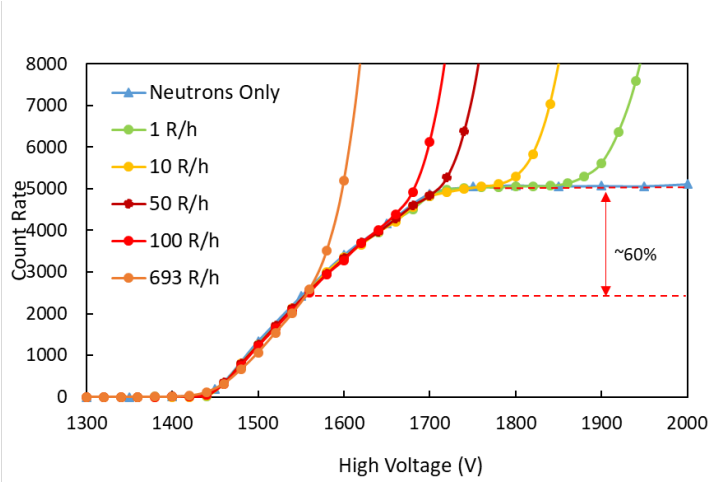

Figure 12: High-voltage plateau of ^{3}He detector ^{3}He_1 without lead brick for a mixed neutron and gamma source term at various gamma-ray dose rates.

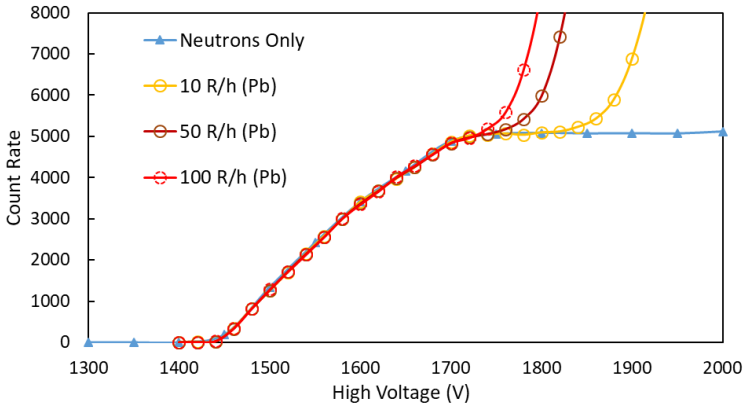

Figure 13: High-voltage plateau of ^{3}He detector ^{3}He_1 with lead brick for a neutron and gamma source at various gamma-ray dose rates.

Figures 12 and 13 show the neutron detection performance of detector ^{3}He_1 (4 atm) in various gamma dose rates using HV plateau curves in the presence of neutron and gamma sources. This is accompanied by Table 7, which quantifies the reduction in neutron detection efficiency for the available gamma dose rates as well as reduced operating HV setting required to tolerate each gamma dose rate. Note that the standard optimum HV setting for this detector corresponds to 1760 V. Results in Table 7 were calculated for each gamma dose rate, by obtaining the neutron count rates corresponding to the point before the neutron signal begins to be affected by gamma pile-up.

From Figure 12 it can be seen that no HV reduction is needed for dose rates of 1 and 10 R/h and neutron detection performance begins to be affected at 50-100 R/h for unshielded 4 atm ^{3}He detector. When a 2" thick lead brick is added to the front face of the detector the performance of 4 atm ^{3}He detector is extended to ~100 R/h with minimum impact on neutron detection performance, however at the expense of added weight (Figure 13).

Table 7. Neutron count rate for 4 atm ^{3}He detector (^{3}He_1) at various gamma dose rates available in this evaluation.

Gamma Dose Rate [R/h]	High Voltage [V]	Neutron Count Rate [cps]	σ [cps]	Percent Reduction of Neutron Detection Efficiency [%]
1	1840	5071	23	-
10	1760	5040	22	-
50	1700	4850	22	4
100	1640	4018	20	21
693	1540	2014	14	60

Similar experiments were performed using the second ^{3}He detector (detector ^{3}He_2), which was pressurized at 9 atm. In this case, fewer measurements were performed as the effects of loss in neutron detection efficiency were apparent at lower gamma dose rates compared to the detector ^{3}He_1 as expected given the detector ^{3}He_2 higher fill gas pressure. Results of these measurements are summarized in Figure 14 and Table 9. When increasing the gamma dose rate from 1 R/h to 50 R/h, there is a 15% decrease in neutron detection efficiency as seen in Table 8. Using the 4 atm detector, for the same conditions, the decrease was only ~4% as shown in Table 7. However, comparing the neutron count rates in Table 7 and 8 it can be seen that at 50 R/h, ^{3}He_2 still provides slightly higher neutron detection performance than detector ^{3}He_1.

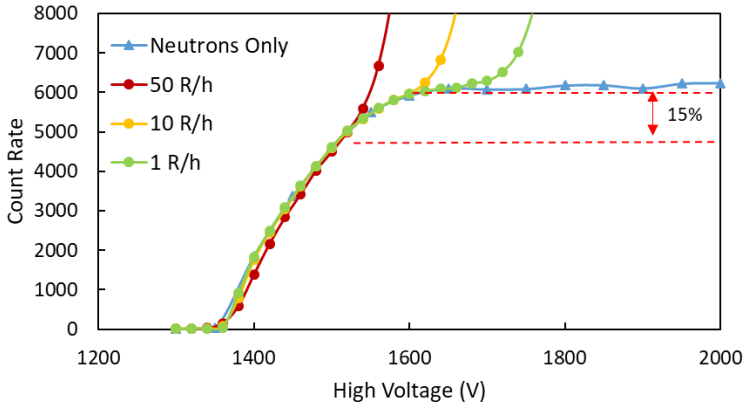

Figure 14: High-voltage plateau of detector ^{3}He_2 for a neutron source and various gamma-ray dose rates.

Table 8. Neutron count rate for 9 atm ^{3}He detector (^{3}He_2) at various gamma dose rates available in this evaluation.

Gamma Dose Rate [R/h]	High Voltage [V]	Neutron Count Rate [cps]	σ [cps]	Percent Reduction of Neutron Detection Efficiency [%]
1	1660	6114	25	-
10	1600	5957	24	3
50	1520	5039	23	15

Looking at detection performance of the miniHDND in Figure 9, it is seen that miniHDND is capable to tolerate a large increase (10 R/h to 693 R/h) in gamma dose rate with only ~26% reduction in neutron detection performance. To compare that with detector ^{3}He_1 in Figure 12 (Table 7), similar decrease in neutron detection performance (~21%) is noticed but at a much lower gamma dose rate of 100 R/h. Hence, the miniHDND can tolerate gamma dose rates of ~700 R/h with 24% neutron detection efficiency reduction, whereas the unshielded 4 atm ^{3}He can only operate at 100 R/h with the same relative neutron detection efficiency performance. Nevertheless, neutron count rate corresponding to 693 R/h for miniHDND is 1931 ± 14 cps, which is comparable to neutron count rate observed for the ^{3}He detector at this dose rate, which corresponds to 2014 ± 14 cps. Both systems in the current configuration provide comparable neutron detection performance at ~700 R/h, however, in case of the ^{3}He detector at the expense of non-optimum HV setting. To operate at this gamma dose rate, ^{3}He requires HV setting far off the plateau and would therefore be prone to count rate variations and instabilities due to minor fluctuation in HV. Thus, in high gamma dose environments, miniHDND would provide a more reliable performance. Additionally, as will be described in Section 4.1, miniHDND is capable to extend neutron counting capability to significantly higher gamma dose rates than ^{3}He.

Lastly, the same experiments were performed using a fission chamber detector. The fission chamber was placed inside the same polyethylene holder and insert as the ^{3}He detectors. A ^{252}Cf source was taped to the holder and was raised on a source stand. The detector was evaluated under the same gamma dose rates between 10 R/h and ~700 R/h. The results are summarized in Table 9.

Table 9: Neutron detection count rates for a fission chamber at various gamma dose rates.

Dose Rate [R/h]	Neutron Count Rate [cps]
0	99.6 ± 0.5
500	99.4 ± 0.5
693	100.0 ± 0.8

The results confirm that fission chamber neutron detection performance is unaffected by gamma dose rates available in these measurements. However, an apparent disadvantage is the low neutron detection efficiency demonstrated in measured count rates of ~100 cps compared to ~2000 cps from ^{3}He and miniHDND exposed to similar gamma dose rates.

4.1. ^{3}He and miniHDND performance for extrapolated high dose rates

The above evaluation demonstrated a very good capability of miniHDND to withstand high gamma dose environments with modest reduction in neutron detection efficiency with additional room for further gamma dose rate increase. Selected ^{3}He tubes provided comparable performance, however at the expense of significant reduction of HV, which requires operating the detectors deep in the HV curve rising edge and would have practical implications on long term measurement stability prone to fluctuations in HV supply. Furthermore, additional increase of gamma dose would result in loss of neutron detection performance in ^{3}He. Trends in Figures 9 and 12 can be used to extrapolate ^{3}He and miniHDND performance to dose rates beyond the values available in the current measurements. Such extrapolation is shown in Tables 10 and 11 where count rates obtained from the experimentally measured HV plateaus for gamma dose rates up to 693 R/h are used to extrapolate to higher dose rates and neutron count rates. These tables provide a valuable indication of expected miniHDND and ^{3}He performance at gamma dose rates above ~1000 R/h, expected in MSR environment. As expected, based on the principles of miniHDND detection, miniHDND neutron detection capability will overcome that of ^{3}He at very high dose rates. Tables 10 and 11 suggest that at ~1500 R/h miniHDND neutron count rate will be ~20% higher than that from a ^{3}He tube and at ~3000 R/h miniHDND will provide a factor of 2 higher neutron detection efficiency than 4 atm ^{3}He detector. This is the key capability of miniHDND, which will be essential for very high gamma dose environments expected in MSR applications.

Table 10: MiniHDND with extrapolated values of dose rates, high voltage setting and corresponding neutron count rates.

Gamma Dose Rate [R/h]	High Voltage [V]	Neutron Count Rate [cps]	σ [cps]
100	940	2317	15
693	880	1931	14
1000	876	1957	14
1500	873	1941	14
3000	853	1836	14

Table 11: ^{3}He with extrapolated values of dose rates, high voltage setting and corresponding neutron count rates.

Gamma Dose Rate [R/h]	High Voltage [V]	Neutron Count Rate [cps]	σ [cps]
100	1640	4018	20
693	1540	2014	14
1000	1547	2073	14
1500	1530	1621	13
3000	1450	773	9

5. Realistic Spent Fuel Measurement Campaign

To enable a comprehensive assessment of the selected neutron NDA technologies in spent fuel measurement applications, a dedicated measurement campaign was conducted at the Oak Ridge National Laboratory (ORNL) Irradiated Fuels Examination Laboratory (IFEL). This campaign provided a unique access to realistic commercial reactor spent fuel materials. Although the general characteristics of this material differ from that of a MSR fuel salt (solid, UO_2 fuel rods after substantial cooling time as opposed to liquid, UF_4 bearing spent fuel freshly removed from a reactor), such measurements present a unique opportunity to perform neutron assay in realistic background environments using rarely accessible spent fuel samples. The goal of these measurements was to evaluate the neutron instruments under high background (neutron as well as gamma) conditions with realistic gamma-ray emissions from spent fuel material.

Spent nuclear fuel rods available at ORNL offer an opportunity to evaluate neutron NDA measurement performance with realistic, high activity materials [8]. The rods came from fuel assemblies irradiated at the North Anna Power Station and were shipped to ORNL in 2016. Rod average burnup is greater than 45 GWd/MTU and documented discharge dates range from 1994-2010. Some of the fuel rods were undergoing processing and were cut into 5" length segments available for neutron measurements. An overview of the rod segments used in the neutron measurements is shown in Table 12. Table 12 also lists gamma dose rates that were measured by the ORNL personnel in the configuration corresponding to neutron measurements. Five rod segments were measured using miniHDND and ^{3}He detectors. Reduced number of measurements was performed with fission chamber, due to the low neutron detection efficiency, as explained in Section 5.4. Only the 4 atm ^{3}He detector (^{3}He_1) was used in these measurements, since it provides higher gamma dose tolerance, as shown in Section 4, and would therefore be more suitable for this type of application. It should be noted that the total mass of the rod segments available at IFEL corresponds to ~120 g of UO_2 with Pu content of ~1-1.5 g. For comparison, the Pu content in 100 g of MSDR salt, which can be extracted based on the SCALE calculations discussed in Section 2, corresponds to ~0.5 g of Pu. It can be expected that there will be substantially higher contribution from (α,n) reactions in MSR-like material, however, the present measurements using spent fuel rod segments provide a representative Pu (and Cm) content.

Table 12: Summary of spent fuel rod segments characteristics, used for neutron measurements at the ORNL Irradiated Fuels Examination Laboratory.

Item	Dose rate [R/h]	Burnup [GWd/MTU]	Cooling Time [Years]
Item 1	208	64	21.2
Item 2	140	49	32.3
Item 3	144	57	26.7
Item 4	192	59	17.1
Item 5	244	57	10.7

The unique aspect of these measurements was that the individual neutron detection technologies were introduced into the hot-cell via a dedicated collimator port. This enabled access to realistic neutron and gamma-ray background conditions inside the hot-cell without contaminating the instrumentation. A photograph of the experimental location at IFEL is shown in Figure 15. Figure 16 shows a diagram of the collimator configuration and detector set-up. The detectors were inserted into the collimator opening and

were positioned at the far end of the collimator port, well inside the hot-cell area. To enable such configuration and simultaneously assure sufficient neutron moderation, dedicated polyethylene detector insert and rod segment holder were designed and fabricated at LANL based on the ORNL provided design drawings. The goal was to assure stable and reproducible positioning of the individual detectors inside the collimator port as well as reproducible positioning of the individual rod segments, while providing necessary neutron moderation. The design and photographs of the finished polyethylene insert and rod segment holder are shown in Figures 17-19.

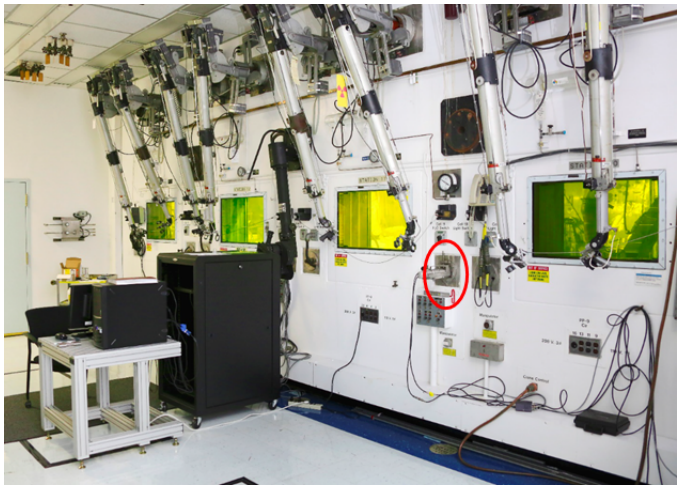

Figure 15: (From ORNL/SPR-2017/535) Photograph of the wall of the east cell bank. The two windows on the right-hand side of the photograph surround the port where the measurements were performed.

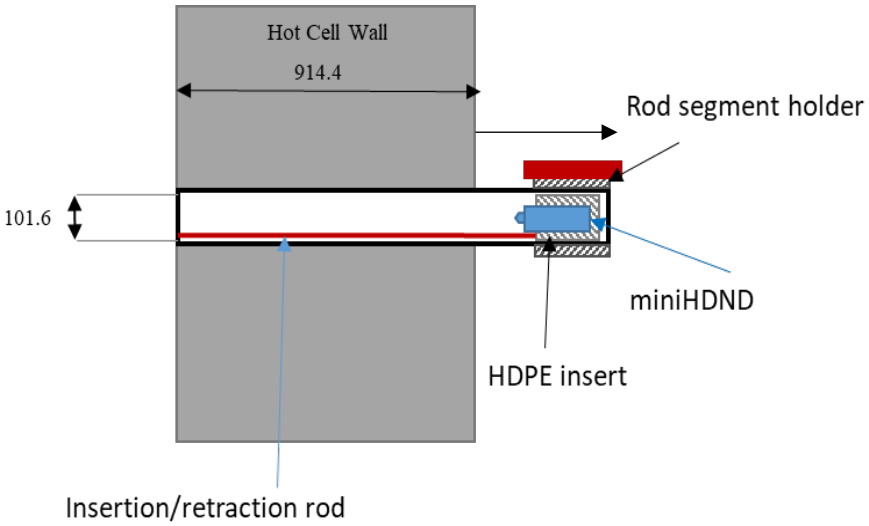

Figure 16: Diagram of the measurement geometry with the miniHDND detector placed inside an IFEL hot-cell collimator port. Dimensions are in mm.

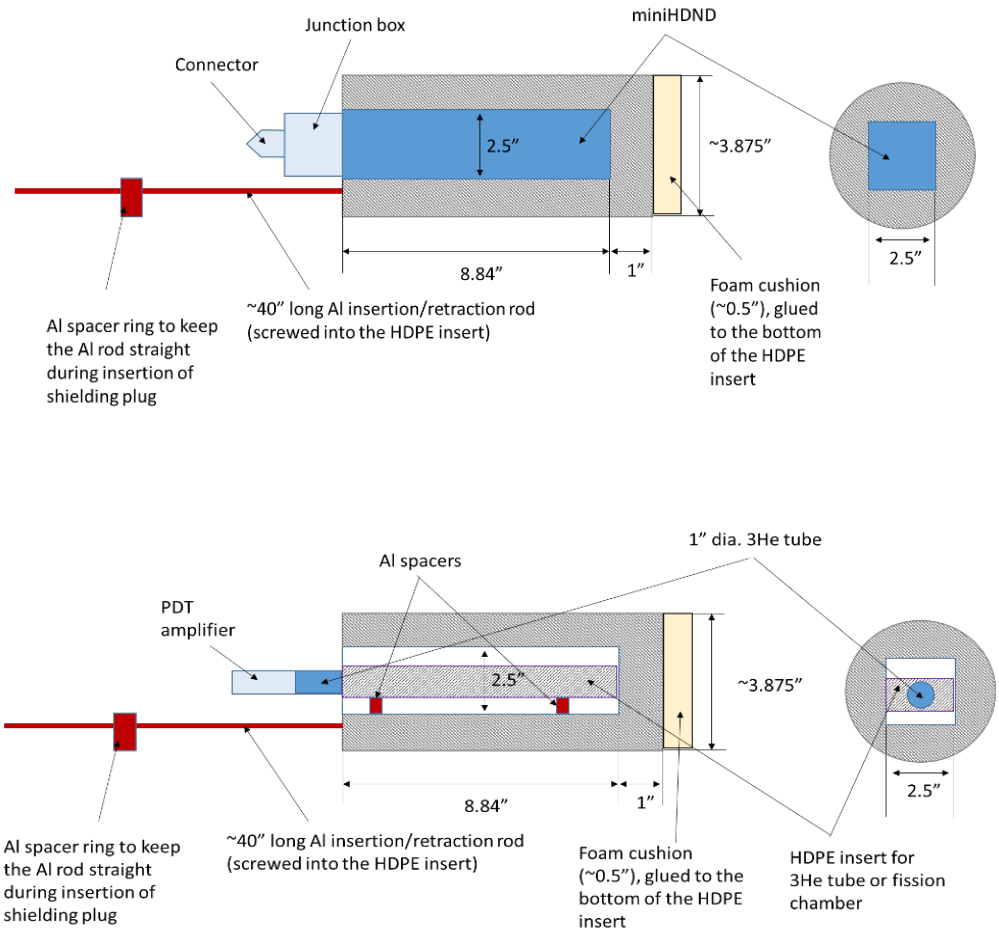

Figure 17 Detailed drawings of the polyethylene insert for the detector insertion into the collimator port; (top) miniHDND; (bottom) ^{3}He or fission chamber.

Figure 17 shows a detailed layout of the detector insert. The insert fits within the cavity of the collimator (shown in Figure 16). The insert has a ~3.9” diameter footprint in order to fit within the 4” internal diameter of the collimator port. Additionally, a retractor rod was attached to the polyethylene insert to aid with insertion and removal of the system within the collimator port. A single insert was manufactured and used to hold the miniHDND and the tube detectors (^{3}He detector and fission chamber, as shown in Figure 18). Additionally the original rectangular polyethylene insert with 1” diameter opening, described in Section 3 and shown in Figure 17 bottom and Figure 18, was utilized for the tube detectors. This was to ensure that all the detectors were directly comparable and had the same amount of polyethylene and to account for the polyethylene structurally embedded within the miniHDND. Finally, a cadmium sleeve was used for the ^{3}He detector and fission chamber to maintain consistent active length.

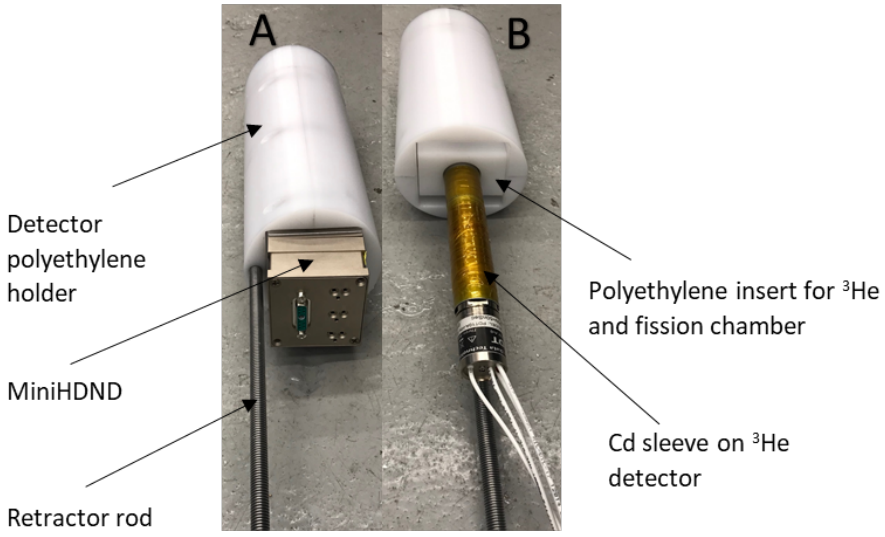

Figure 18: Photograph of the finished polyethylene holder to slide inside the collimator port with the (A) miniHDND and (B) ^{3}He detector inserted. Note the additional polyethylene insert and Cd sleeve for ^{3}He.

Figure 19 shows the polyethylene rod segment holder that was manufactured to be placed inside the hot cell around the external part of the collimator and to hold the rod segment while providing additional neutron moderation. A 8“ long aluminum wedge was attached by screws to the holder to hold the rod segments to ensure reproducible positioning between experiments and allow for easy rod segment insertion and removal using remote manipulators. The polyethylene ring has a 5” internal diameter and is 1” thick. It was designed with a hinge to open up and be secured in place with a dedicated screw attached to the assembly so that it does not fall out in the hot cell during manipulation. A rubber sleeve (visible in Figure 19 (A)) was attached to the inside of the holder to prevent it from slipping when secured on the collimator port. Figure 20 shows this setup mounted inside the hot cell. While the detector insert as well as the individual detectors remained separated from the hot cell environment by the collimator wall, the rod segment holder had to be introduced directly inside hot cell and due to contamination was not retrieved at the end of the measurement campaign.

Figure 19: Polyethylene holder with aluminum wedge to hold rod segments; (A) front view and (B) top view.

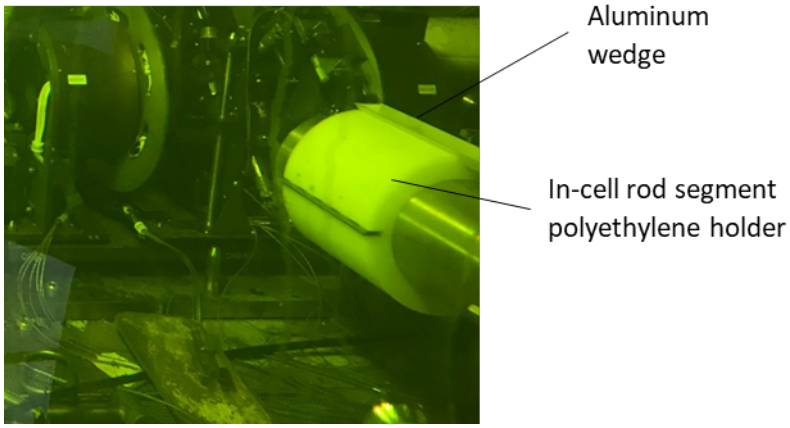

Figure 20: Photograph of setup inside hot cell depicting the rod segment polyethylene holder and aluminum wedge attached to the in-cell portion of the collimator.

The insertion of miniHDND into the collimator opening is shown in Figure 21. It can be seen that the miniHDND was oriented with cells facing (parallel to) the rod segment holding wedge positioned on top of the collimator. The first miniHDND cell (near cell) was therefore located closest to the rod segment, while the third cell (far cell) was located farthest away from the rod segment (for internal structure of miniHDND refer to Figure 6). After each detector was inserted into the collimator port, a dedicated shielding (shown in the left part of Figure 21) was inserted to prevent any radiation streaming through the opening.

Figure 21: Photograph of insertion of miniHDND in polyethylene insert into the collimator opening at IFEL hot cell.

5.1. Measurement Procedure and Background Conditions

For adequate evaluation of neutron technology performance for the available spent fuel rod segments, a dedicated measurement procedure was developed to assure appropriate operating setting was established for each detector. As discussed in Section 4, neutron detection performance of each detection technology (with the exception of fission chamber) is strongly dependent on the gamma background environment. Since this campaign was focused on measurements of spent fuel, the first goal was to establish the appropriate operating high voltage suitable for gamma dose rates from the available rod segments. To extract operating high voltage a high voltage plateau was measured for the rod segment with the highest gamma dose rate. The ORNL personnel measured the gamma dose rates for each rod segment positioned in the rod segment holder, in the configuration corresponding to the neutron detectors inside the collimator port. The corresponding dose rates are summarized in Table 12.

Additionally, background gamma dose rate was measured with no rod segments present in the holder. Since there are significant amounts of nuclear material present inside the hot cell, high neutron and gamma-ray backgrounds at the collimator location can be expected. The background gamma dose rate measurement indicated dose rate of 64 R/h inside the collimator, in the detector position, with no rod segments present. As can be seen from Table 12, the dose rates from the individual fuel rod segments are about 2-3 times this value. Overall, the gamma dose rates encountered at IFEL are lower than those evaluated at LANL RIC facility and lower than expected for MSR applications. This can be expected, due to the long cooling times of the available rod segments. However, in addition to gamma-ray background, high neutron background is also present inside the hot cell as will be further discussed in the following sections. As such the IFEL measurements present a unique opportunity to perform measurements under near-realistic background conditions.

Based on the high voltage plateau measurement an optimum operating high voltage was established for miniHDND and ^{3}He detector, which was used throughout the remainder of the measurements. To compare performance of the three neutron detection technologies, each rod segment was measured for 300 – 3000 s to obtain sufficient statistics. Additionally, process monitoring capability was evaluated via continuous data recording during rod segment exchanges between the measurements. The results of these measurements are summarized in the following sections.

5.2. Results and Discussion for MiniHDND

MiniHDND offers capability to simultaneously measure neutron and gamma-ray signals via signal collection from each of its three cells individually. During the IFEL measurements the data from miniHDND was collected in list mode for each cell (2 neutron cells and one gamma cell) separately. The neutron count rates and high voltage plateaus reported here correspond to sum of signals from the 2 neutron cells. The gamma count rates were recorded on the middle cell, which is not boron coated. Note that the gain of the middle cell was pre-set to a slightly higher gain than for the neutron cells for these measurements. This assured that the middle cell was sensitive to gamma pile-up even at the optimum operating high voltage selected to prevent any gamma interference on the two neutron cells. Such hardware

implementation enables simultaneous neutron and gamma-ray measurement capability at a single HV setting. More details about this concept of electronics gain adjustment can be found in [4].

As discussed above, HV plateau measurements were performed in order to establish miniHDND response to gamma dose from the spent fuel rod segments and establish operating voltage for neutron measurements. Each of the five rod segments were measured one at a time and were placed flush with one side of the 8“ aluminum wedge on the rod segment holder to ensure reproducible positioning. The measured HV plateaus for the miniHDND are shown in Figure 22. It can be seen that onset of gamma signal is noticeable at HV above ~960V for the highest gamma dose fuel segments. The operating voltage for the subsequent measurements was therefore selected as 960 V to minimize gamma contribution to the neutron signal. Additionally, for comparison, the ^{252}Cf neutron HV plateau obtained in Section 4 is also included in Figure 22 (black points, referred to as LANL RIC Neutrons) to better illustrate the onset of gamma pile-up in the fuel rod segment measurements.

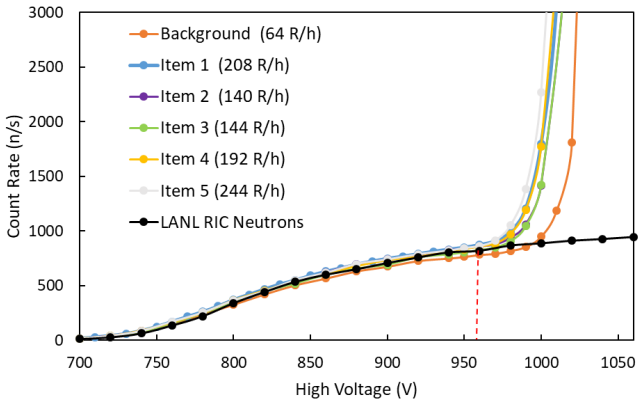

Figure 22: High voltage plateaus for miniHDND neutron cells from all the rod segments and reference ^{252}Cf neutron plateau.

Neutron background measurements were performed with no rod segments present using the miniHDND. The neutron background was considerably high within the hot cell, measuring 749.39 ± 2.08 cps. The measured gamma count rate in the background mode (corresponding to 64 R/h) was 20.91 ± 0.57 cps. For all data shown below, background subtraction was performed. Table 13 shows the neutron and gamma count rates at 960 V for Items 1-5 and Figure 23 shows the gamma count rate at 960 V as a function of gamma dose rate.

Table 13: Neutron and gamma count rates from the miniHDND for all items measured at 960 V.

	Operating HV = 960 V				Burnup [GWd/MTU]	Cooling Time [Years]
	Gamma Count Rate [cps]	σ	Neutron Count Rate [cps]	σ		
Item 1	43.68	0.26	92.04	3.00	64	21.2
Item 2	21.43	0.31	75.27	3.04	49	32.3
Item 3	22.00	0.25	39.83	2.99	57	26.7
Item 4	41.75	0.32	72.92	3.01	59	17.1
Item 5	75.64	0.69	83.2	3.00	57	10.7

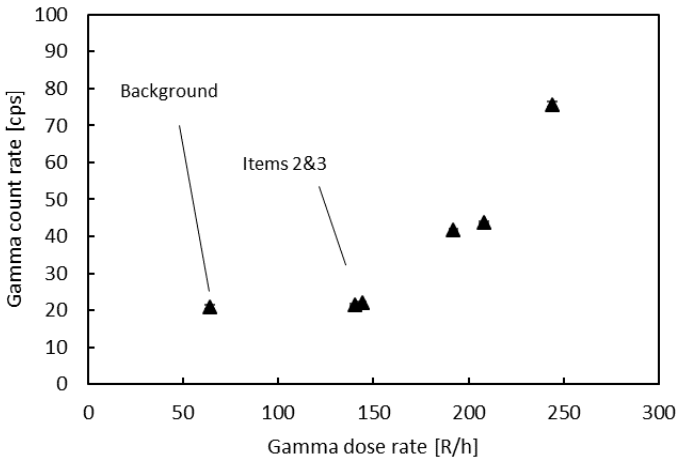

Figure 23. Gamma count rate measured by miniHDND with HV setting of 960 V as a function of dose rate.

Table 13 shows that the net neutron count rates from the available rod segments vary in the range of 40 – 90 counts per second. Note that these are net count rates measured in the presence of significant neutron background (749.39 ± 2.08 cps). Measurement times of 500 s were used to obtain the listed uncertainties. The Pu content of these rod segments is estimated on the order of 1-1.5 g. These measurements therefore illustrate miniHDND capability to reliably distinguish and measure neutron signal on the order of only ~10% of the overall neutron background for gram quantities of Pu in 10 – 30 years cooled spent fuel.

Table 13 and Figure 23 also summarize detected gamma count rates for the 5 rod segments at 960 V. From Figure 23 it can be seen that measured gamma count rates exhibit expected trends with increasing gamma dose rate. Note however, that at this high voltage setting items 2 and 3 do not result in sufficient gamma count rate to be distinguishable from background. These items have the longest cooling times and lowest gamma dose rates. In order to be able to reliably measure the gamma count rate from these items, higher high voltage setting would be necessary for the miniHDND middle cell. To illustrate this, we

performed an additional measurement with the miniHDND middle cell at high voltage corresponding to 980V. The results of these measurements are summarized in Figure 24, which demonstrates a clear dependence of the measured gamma count rate on gamma dose rate. This serves as a demonstration of miniHDND to provide an independent dose rate information, once properly calibrated. Note that an increase in high voltage will not be necessary in practical measurements, since the amplifier gain on the middle cell can be adequately increased for given measurement conditions to provide sufficiently high gamma response at a fixed high voltage used simultaneously for neutron measurements.

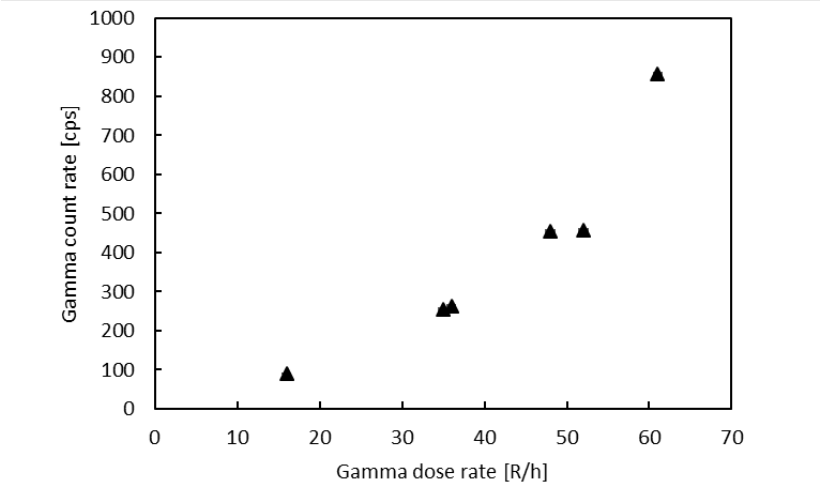

Figure 24. Gamma count rate measured by miniHDND with HV setting of 980 V as a function of dose rate.

Typically, in gross gamma measurements of spent nuclear fuel, the largest contributor to the signal is from ^{137}Cs, which builds up with increasing burnup and decays with increasing cooling time. With the 5 rod segments measured, there is a combination of burnups and cooling times that are available. Figure 25 shows the measured gamma count rates of the fuel segments as a function of cooling time at 980 V. The item with the shortest cooling time is Item 5, and it has the second highest burnup (57 GWd/MTU) among the selection of fuel rod segments. This item provides the highest gamma signal as many long-lived fission products and actinides have built up with the high burn up and have not decayed, especially ^{137}Cs which has a half life of 30.17 years [2]. This figure demonstrates that measured gamma count rate decreases proportionally as a function of cooling time.

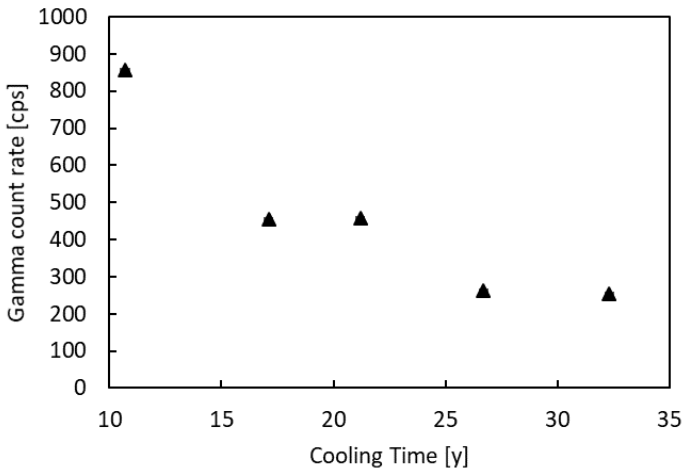

Figure 25. Gamma count rates measured by miniHDND for the set of 5 fuel rod segments as a function of cooling time at 980 V.

While there is an apparent scaling between cooling time and gamma ray signal, the observation is more convoluted for neutrons. The main contributors to neutron signal are from the combination of Plutonium and curium isotopes (specifically from ^{244}Cm for cooling times in this campaign). These isotopes build up with burnup but have much longer half-lives than available cooling time. Figure 26 depicts the neutron count rate as a function of burnup for reference. In Figure 26, a trend is noticed, for the same burnup, the item with the lowest cooling time has the higher neutron count rate. This is true for items 3 and 5, depicted in the red box, where item 5 has the shorter cooling time of 10.7 years instead of 26.7 years of item 3. However, in general the rod segments represent a combination of burnups and cooling times and to perform a further analysis of the measured neutron signal, additional knowledge of the isotopic composition of the fuel rods would be required, which is currently not available. We will coordinate with ORNL to obtain additional information as it becomes available to enable further interpretation.

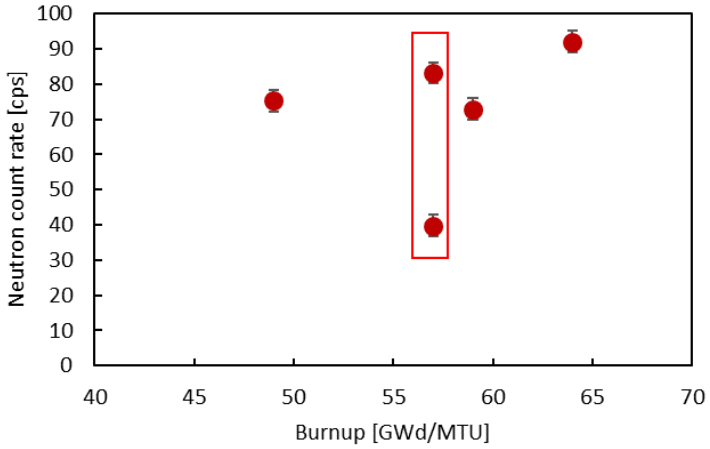

Figure 26: Neutron count rate at 960 V as a function of burnup.

Nevertheless, as discussed earlier, the key contribution of these measurements lies in the demonstration of miniHDND capability to perform reliable neutron detection of gram quantities of Pu in challenging neutron and gamma-ray background environments. Using the miniHDND to measure fuel rod segments

allowed for field testing to be done with the most realistic spent nuclear fuel available. It is reiterated here that the miniHDND has the capability to monitor neutron and gamma rays within the same measurement, in the presence of high neutron and gamma-ray backgrounds. This field test serves a crucial demonstration to inform the overall capability of neutron NDA for MSR fuel measurements and development of future safeguards approaches.

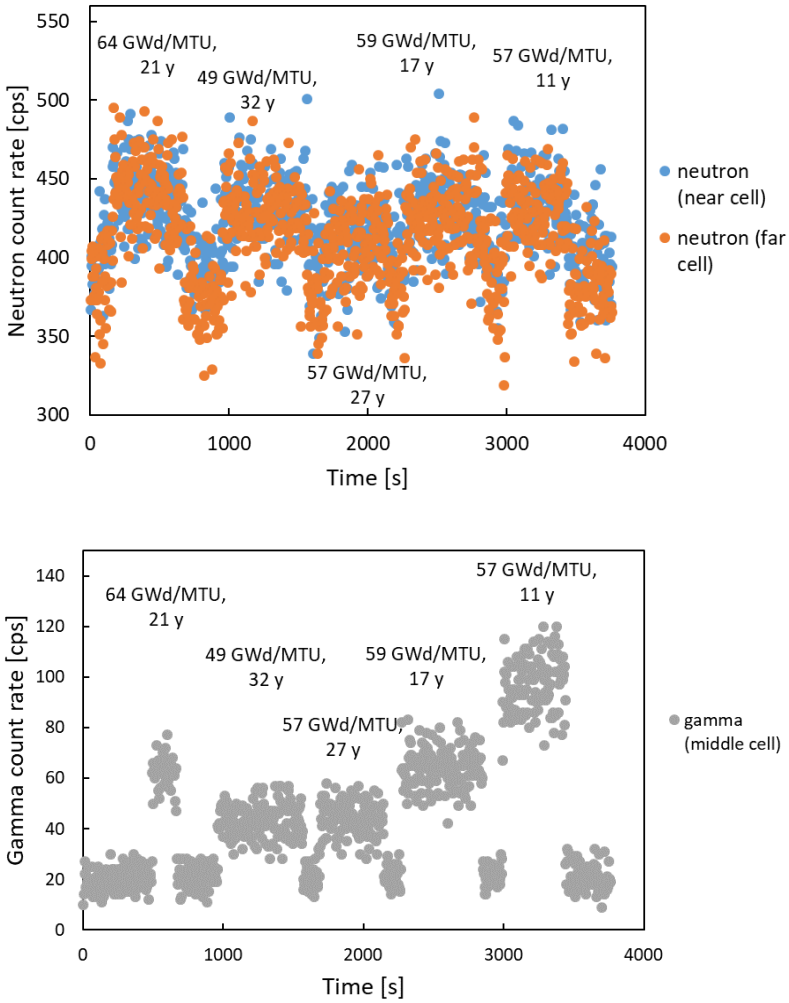

Figure 4: MiniHDND process monitoring capability for (top) neutrons and (bottom) gamma rays as a function of time.

Additionally, the miniHDND could also be used for process monitoring. This is the ability to take continuous measurements and decipher if there is movement of nuclear material. To test this, 1 second measurements were taken during replacing rod segments, i.e. when moving from Item 1 to Item 2 and so forth. The neutron and gamma count rates obtained during the monitoring periods were extracted and the results are shown in Figure 27. Using this detector for neutron measurements, it can be seen that there are increases and decreases in count rate that indicate the presence and absence (moving) of a neutron source. Signals from both of the miniHDND neutron cells are shown separately. Note that monitoring these two cells can also provide information on direction of motion, as demonstrated in [9]. Near cell refers to cell within the miniHDND located closest to the rod segment. Additionally, Figure 27

(bottom) shows the gamma process monitoring capability of the MiniHDND. The gamma-ray signatures provide more insight into the item being measured as items can be discriminated based on their gamma emissions, which were shown to be correlated with the rod segment cooling times. Fuel that has high burnup and short cooling time will have higher gamma emission than fuel with low burnup and long cooling times. In practice, if the miniHDND is calibrated for given measurements, this information could be used to verify/confirm the items being moved via process monitoring.

5.3. Results and Discussion for ^{3}He detector

The same measurements as for miniHDND were performed using a ^{3}He detector, pressurized to 4 atm to provide a complete assessment of neutron detection performance. The ^{3}He detector was placed into the same polyethylene holder as miniHDND and was held in the dedicated insert to ensure the detector maintained its position and to compensate for the additional polyethylene moderator present inside the miniHDND. Additionally a 1 mm thick cadmium sleeve was placed on the top of the detector to ensure consistent active length. Figure 28 shows the setup with the ^{3}He detector being inserted into the collimator opening where the retractor rod is used to position the setup into the hot cell.

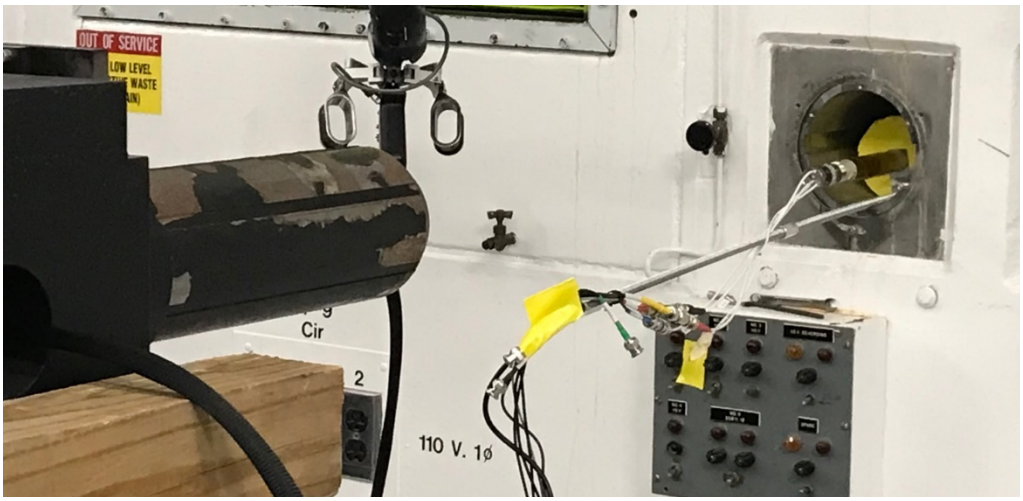

Figure 28. Setup with the ^{3}He detector being inserted into the collimator port.

The first measurement performed was the HV plateau to determine the operating voltage and the results are shown in Figure 29. It can be seen that onset of gamma signal is noticeable at HV above 1680 V for the fuel rod segments. The operating voltage for the subsequent measurements was therefore selected as 1680 V to minimize gamma contribution to the neutron signal. Additionally, for comparison, a scaled ^{252}Cf neutron HV plateau measured at the LANL RIC facility (see Section 4) is also included (referred to as LANL RIC Neutrons in the figure) to better indicate the onset of gamma pile-up from the rod segments in comparison with bare neutron signal.

Neutron background measurements were performed with no rod segment present in the holder using the ^{3}He detector. The neutron background was considerably high within the hot cell, measuring 1670.5 ± 0.2 cps. For all data shown below, background subtraction was performed. Following that, 500 - 1000 s measurements were performed for each of the five rod segments. The results are shown in Table 14.

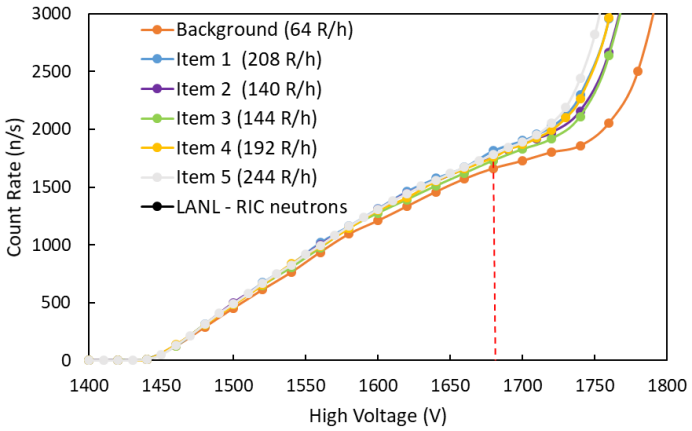

Figure 29: HV plateaus for each of the items measured by ^{3}He detector.

Table 14. Neutron count rates measured by ^{3}He detector at 1680 V.

	Burnup [GWd/MTU	**Cooling Time [Years]**	**Neutron Count Rate [cps]**	**σ**
Item 1	64	21.2	133.6	1.2
Item 2	49	32.3	108.8	1.3
Item 3	57	26.7	58.0	1.3
Item 4	59	17.1	103.5	1.9
Item 5	57	10.7	113.2	1.8

From Table 14, the neutron count rates measured by the ^{3}He detector are on average ~40% higher than those observed by the miniHDND. This is consistent with relative neutron detection efficiencies of these two detectors. Similarly as in case of miniHDND, the ^{3}He measurements have to accommodate the very high neutron background within the hot cell, where the net neutron signal from the rod segments represents only ~10% of the background. Nevertheless, due to the higher neutron detection efficiency than miniHDND, ^{3}He detector is also capable to reliably perform neutron measurements under these conditions. It should, however be noted that the current measurements do not extend into the gamma dose rates representative of MSR applications, where ^{3}He detector performance would be further affected, as demonstrated in Section 4. Since ^{3}He detectors lack the ability to perform simultaneous neutron and gamma measurements, only results using neutron measurements are presented.

The ^{3}He detector could also be used for process monitoring where 1 second measurements were taken in between replacing rod segments, i.e. when moving from Item 1 to Item 2 and so forth. The neutron count rates obtained during the monitoring periods were extracted and the results are shown in Figure 30. Note that only 4 rod segments, as shown in Figure 30, were included in the process monitoring measurements for ^{3}He. In this case, trends are noticed where increases and decreases in count rates can be used to distinguish presence and absence of a neutron source. However, each item can be only barely distinguished from each other based on the neutron count rates only. This information is still highly valuable and can be used at a facility to monitor the processes to verify declarations of item movements.

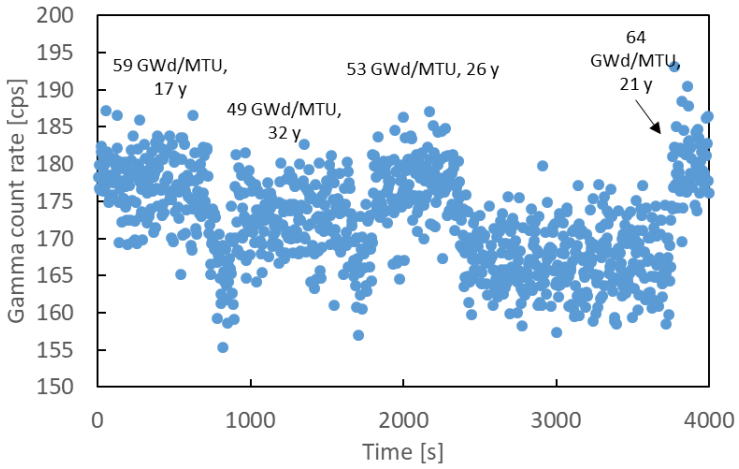

Figure 30: Process monitoring capability of ^{3}He detector.

5.4. Results and Discussion for a fission chamber

The fission chamber possesses the unique ability to withstand high gamma exposures while performing neutron measurements. However a disadvantage of using this detector is that it has very low neutron detection efficiency. The same setup as the ^{3}He detector was used for the fission chamber.

An overnight background measurement was performed to assure sufficient statistics and the neutron count rate observed was 32.9 ± 0.03 cps. Only two rod segments were measured with fission chamber due to the low neutron detection efficiency and low count rate measured from the available material. When using the fission chamber to measure Items 1 and 5, measurement times of 2000 s - 5400 s were needed to be able to statistically distinguish them from background. The net count rates measured were very low as expected from relative fission chamber efficiency compared to the other detectors. Table 15 shows the results of the measurements.

Table 15: Neutron count rates using a fission chamber detector.

Item ID	Dose rate [R/h]	Burnup [GWd/MTU	Cooling Time [Years]	Neutron Count Rate [cps]	σ
Item 1	208	64	21.2	2.64	0.09
Item 5	244	57	10.7	2.13	0.13

While the fission chamber can measure neutrons in the presence of neutron background, the miniHDND and ^{3}He detectors perform at a higher efficiency and produce reliable results under equivalent conditions. The low neutron detection efficiency of the fission chamber is demonstrated in measured neutron count rates of ~2-3 cps compared to ~100 cps from ^{3}He and miniHDND exposed to similar conditions, which renders fission chamber largely unusable for measurement of ~1 gram quantities of Pu present in this material. Note that the total mass of these rod segments is ~120 g of UO_2, which is comparable to item size selected for MSR salt evaluation in Section 2. The Pu content of 100 g of MSDR salt was estimated to correspond to ~0.5 g.

5.5. Summary of Spent Fuel Campaign Observations

The goal of the IFEL measurement campaign was to field test all the detectors with spent nuclear fuel to mimic the conditions expected from MSR fuel. While the items measured in this campaign had lower overall neutron and gamma emission rates than those which would be expected from a MSR material, they provided a unique opportunity to test the capabilities of the detectors in a representative environment. When the detectors were placed within the collimator opening of the IFEL hot cell they were subject to a high neutron as well as significant gamma background. This condition is expected to be analogous to MSR if samples are analyzed proximal to the flow of material, where high neutron and gamma background will be observed.

A summary of the background subtracted neutron count rates are shown for all the detectors in Table 16. ^{3}He detectors possess the advantage of high neutron detection efficiency and measures the highest neutron count rates among all the detectors. However, as demonstrated in Section 4, when placed in a high gamma background, these detectors suffer considerably due to their sensitivity to gamma radiation. For the spent fuel rod segments available in this campaign, ^{3}He would, nevertheless provide a reliable neutron detection capability.

From Table 16, it can be seen that the neutron count rates obtained by the miniHDND are approximately 40% less than those of the ^{3}He detector due to its lower neutron detection efficiency, however, the ability to simultaneously monitor gamma rays and neutrons, along with the ability to withstand high gamma doses with minimal loss to neutron detection (Section 4) allow for the miniHDND to be a viable technique for safeguarding MSR fuel.

The results for fission chamber indicate that it would be difficult to use this technique for measurements of small samples of spent fuel material, due to the very low neutron detection efficiency. The required measurement times to obtain reliable results, would be in excess of 1 hr.

Table 16: Neutron count rates for MiniHDND, ^{3}He and fission chamber detector measured for the spent fuel rod segments available at IFEL.

Item ID	Dose rate [R/h]	Burnup [GWd/MTU]	Cooling Time [Years]	MiniHDND		^{3}He		Fission Chamber	
				Neutron Count Rate [cps]	σ	Neutron Count Rate [cps]	σ	Neutron Count Rate [cps]	σ
1	208	64	21.2	92.04	3.00	133.6	1.2	2.64	0.09
2	140	49	32.3	75.27	3.04	108.8	1.3	-	-
3	144	57	26.7	39.83	2.99	58.0	1.3	-	-
4	192	59	17.1	72.92	3.01	103.5	1.9	-	-
5	244	57	10.7	83.2	3.00	113.2	1.8	2.13	0.13

6. Summary of Neutron NDA Comparison

The focus of this work was to perform a comprehensive evaluation of representative neutron NDA technologies to assess their suitability for development of safeguards for MSR fuel cycle. The MSR reactor implementation, selected for this evaluation is liquid salt fueled MSR with low enriched Uranium in Fluoride salt. A case study of MSDR reactor was used to assess expected neutron and gamma emission characteristics of such material for a representative 100 g salt sample at the end of the 8 year lifecycle of the reactor. It was found that total neutron emission rate (from fission as well as (α,n) reactions) after 8 years of reactor cycle corresponds to ~5.0e5 n/s. In terms of underlying contributions to this neutron emission, the (α,n) reactions will provide the dominant neutron emission contribution (approximately 2 orders of magnitude higher than from fission). Additionally, correlated fission signatures from Pu are largely masked by contribution from ^{242}Cm. This will significantly complicate neutron assay of this type of material.

Additionally, understanding gamma emissions will be essential in order to evaluate the useability of neutron detection techniques, since neutron detection will need to be performed in very high gamma backgrounds. Neutron detectors are, to a varying degree, prone to gamma pile-up. An initial estimate suggests that gamma dose rates from 100 g of MSDR fuel salt after 8 years of irradiation, freshly removed from the reactor, will correspond to 1000s of R/h. These are extremely high dose rates that typically require use of additional shielding with ^{3}He detectors or fission chambers.

To perform an assessment of neutron NDA performance under the conditions expected based on the MSDR analysis, series of dedicated measurements was performed. Three representative neutron detection technologies were selected, including standard instruments (^{3}He detectors and fission chamber) and novel boron-line instrument (miniHDND). All these techniques were first evaluated in very high gamma dose rates at LANL RIC facility to establish their performance limits with gamma doses in the excess of 100 R/h. The highest gamma dose rate available at this facility corresponds to ~700 R/h, which

is a very good reference for MSR-type material performance. Measurements at RIC were used to extrapolate the expected neutron detection capability of ^{3}He and miniHDND for higher gamma dose rates, not available at the facility. Overall it was found that ^{3}He can operate up to ~10 - 50 R/h with no major impact on neutron detection performance, after which point a HV reduction will result in reduced neutron detection efficiency and more importantly, operating point outside of the stable HV plateau region. Two ^{3}He detectors were tested, with different fill gas pressures (4 and 9 atm). As expected, the lower pressure detector clearly exhibits superior performance in high gamma background and would, therefore, be more suitable for MSR applications. The 4 atm ^{3}He can tolerate ~700 R/h, even 1000 R/h dose rates, however, at the expense of dramatic reduction in neutron detection efficiency and operation well outside the stable plateau region of HV plateau curve.

Compared to that, miniHDND can operate at ~700 R/h and well above ~3000 R/h with reduced, but still measurable neutron signals. This is a consequence of high energy tail in the pulse height distribution for this type of detection technique. For very high dose rates (>1000 R/h), miniHDND is expected to outperform ^{3}He neutron detection capability.

Fission chamber provides excellent gamma resistance, however at the expense of very low neutron detection efficiency, which, as demonstrated in spent fuel measurements within this work, renders it largely unsuitable for applications that require high neutron detection efficiency.

Following the high gamma dose evaluation, all three technologies were further assessed in a dedicated field test at the ORNL IFEL facility, using realistic spent fuel rod segments. This campaign provided a unique opportunity to assess the technologies in realistic background and facility environments using spent fuel rod segments with Pu content representative of 100 g of MSDR material. The key findings are summarized in Section 5.5 and indicate that both, miniHDND as well as ^{3}He would provide viable approaches for this material. Contrary to that, it was shown that fission chamber measurements become impractical for small samples (~1 g quantities of Pu content) due to the low neutron detection efficiency. Nevertheless, these results need to be extrapolated into high gamma dose rates expected in MSR applications (1000s of R/h), where the boron-lined technology (miniHDND) would provide a distinct advantage due to its lower sensitivity to gamma pile-up. The key result of the spent fuel rod segments measurement campaign was observation that neutron measurements are possible in the challenging neutron and gamma background environments and that both, ^{3}He and miniHDND are capable to measure neutron signals from small samples containing ~1g of Pu at reasonable measurement times (< 1000 s in these conditions). Note that the actual measurement time will depend on neutron background conditions at the MSR facility, but the current results provide a good initial expectation.

Finally, process monitoring capability was evaluated for ^{3}He and miniHDND. Both instruments demonstrated capability to follow and monitor live movement of rod segments as performed by the IFEL hot cell operators. The miniHDND additionally was demonstrated to provide a viable simultaneous neutron and gamma detection capability, which can provide an additional observable to aid in characterization of nuclear material and development of safeguards approaches. The gamma signal from miniHDND was shown to scale with ‘declared’ gamma dose rates as well as cooling time of the measured fuel rod segments. This is a unique capability not available in any of the other neutron detection technologies.

7. FY22 ORNL Measurement Campaign Planning

FY22 measurement campaigns at Oak Ridge National Laboratory will focus on gamma spectroscopy measurements of irradiated fuel materials, in particular dissolved samples that are expected to show X-ray features in the gamma spectrum that are more representative of liquid fuel in an MSR. This includes a series of unusually well-characterized aqueous solution samples that are undergoing destructive analysis in the Building 4501 radiochemistry laboratories (Figure 31 left). This will allow us to extend our evaluation of NDA isotopic characterization techniques to include systematic uncertainty in addition to statistical uncertainty as in previous work. We have selected high-purity germanium and microcalorimeter detectors for this campaign based on FY20 results that show both detector types have specific advantages for different parts of the gamma spectrum. The SOFIA microcalorimeter spectrometer was not available for measurements in FY21 due to its use at the LANL plutonium facility, where measurements were delayed due to factors outside of the team's control. SOFIA measurements at ORNL will be completed in FY22 instead.

A second measurement location at the Radiochemical Engineering and Development Center (REDC) will allow access to the Hybrid K-edge Densitometer (Figure 31 right) which can perform X-ray absorption measurements of uranium and plutonium in solutions using a 160 kV X-ray source. The system will be used with its standard high-purity germanium detector and the SOFIA microcalorimeter detector to measure the absorption and fluorescence signals. These measurements will allow us to evaluate the potential of nondestructive assay based X-ray interrogation of liquid samples representative of liquid fuel salt.

Figure 31: Gamma measurement locations at Oak Ridge National Laboratory will include the Building 4501 radiochemistry laboratory (pictured on left) and the Radiochemical Engineering and Development Center (REDC) Hybrid K-edge Densitometry Laboratory (pictured on right).

8. FY22 INL Measurement Campaign Planning

Idaho National Laboratory is active in the development of pyroprocessing technology and has current programs exploring spent nuclear fuel separations using molten salt technology. Measurements are planned at the Materials and Fuels Complex Analytical Laboratory (AL) to evaluate laboratory NDA of small process samples, and at the Hot Fuel Examination Facility (HFEF) to evaluate on-line measurements. The questions that will be considered by this measurement campaign include:

1. What are the observable signatures of fissile material content available with each measurement technology?
2. How precisely can these signatures be quantified?
3. How can salt samples with fissile material and fission products be handled in a laboratory to achieve optimized NDA measurement performance?

The AL routinely analyzes a wide range of samples from advanced nuclear fuel cycle development work at Idaho National Laboratory, and includes destructive and traditional nondestructive analysis capabilities. Through separate projects, a microcalorimeter gamma spectrometer is currently being built for deployment to the AL by April 2022. This new instrument will be used alongside traditional NDA technologies to measure available samples from electrochemical separations relevant to on-line separations in liquid-fueled MSRs. An important outcome of this measurement campaign will be to validate the performance of advanced and traditional NDA technologies with the same relevant samples handled in a laboratory environment.

9. Acknowledgements

We gratefully acknowledge the support of staff at the ORNL Irradiated Fuels Examination Facility in making the neutron measurement campaign a success, as well as Wade Ivey, Joe Giaquinto, Robert McElroy, and Riley Hunley in planning FY22 gamma measurements. This work is supported by the U. S. Department of Energy, Office of Nuclear Energy, Advanced Reactor Safeguards program.

10. References

1. M. Higgins, N. Shoman, B.B.Cipiti, “Limitations of MUF for MSRs” INMM Annual Meeting Proceedings. Pre-print (2021)

2. D. Reilly, N. Ensslin, H. Smith, Jr., and S. Kreiner, Passive Nondestructive Assay of Nuclear Materials, Los Alamos National Laboratory Technical Report LA-UR-90-732 (1991).

3. W.B. Wilson, R.T. Perry, E.F. Shores, W.S. Charlton, T.A. Parish, G.P. Estes, T.H. Brown, E.D. Arthur, M. Bozoian, T.R. England, D.G. Madland, and J.E. Stewart, “SOURCES 4C: a code for calculating (α,n), spontaneous fission, and delayed neutron sources and spectra (LA-UR--02-1839)” (Jan 2002)

4. D. Henzlova and H.O. Menlove, High-Dose Neutron Detector Development, Los Alamos National Laboratory report, LA-UR-15-27500, 2015.

5. D.H Beddingfield, N.H Johnson, H.O. Menlove, “3He neutron proportional counter performance in high gamma-ray dose environments”, Nuclear Instruments and Methods in Physics Research A 455 (2000), p.670-682

6. H.O Menlove, “AEFC for the Verification of Research Reactor Spent Fuel – Field Experience to Date”. United States: N. p., 2017. Web. doi:10.2172/1344342.

7. A.Trahan, V. Henzl, H.O Menlove, M.T Swinhoe, A.Belian, M. Flaska, S. Pozzi, “Determination of spent nuclear fuel assembly multiplication with the differential die-away self-interrogation instrument”, Nuclear Instruments and Methods in Physics Research Section A Accelerators Spectrometers Detectors and Associated Equipment. 757. 20–27. 10.1016/j.nima.2014.04.023. (2014).

8. R. Montgomery, B. Bevard, “Sister Rod Destructive Examinations (FY20)”. United States. https://doi.org/10.2172/1764465

9. D. Henzlova and H.O. Menlove, Final Report on High Dose Neutron Detector for FY18, Los Alamos National Laboratory report LA-UR-18-29899, 2018.